JGR Oceans

RESEARCH ARTICLE
10.1029/2021JC017524

Moored Observations of the Iceland-Scotland Overflow Plume Along the Eastern Flank of the Reykjanes Ridge

W. E. Johns[1], M. Devana[1], A. Houk[1], and S. Zou[2]

[1]Rosenstiel School of Marine and Atmospheric Science, University of Miami, Miami, FL, USA, [2]Woods Hole Oceanographic Institution, Falmouth, MA, USA

Key Points:

- Dense waters overflowing the Iceland-Scotland ridge nearly double their volume transport through entrainment of lighter ambient waters
- The export of the Iceland-Scotland Overflow Water from the Iceland Basin is approximately 5.3 Sv net of interior recirculation
- The transport of the Iceland-Scotland Overflow plume found in this study is larger than most previously published estimates

Supporting Information:

Supporting Information may be found in the online version of this article.

Correspondence to:

W. E. Johns,
bjohns@rsmas.miami.edu

Citation:

Johns, W. E., Devana, M., Houk, A., & Zou, S. (2021). Moored observations of the Iceland-Scotland Overflow plume along the eastern flank of the Reykjanes Ridge. *Journal of Geophysical Research: Oceans*, *126*, e2021JC017524. https://doi.org/10.1029/2021JC017524

Received 28 APR 2021
Accepted 9 AUG 2021

Abstract Since 2014, an array of current meters deployed in the Iceland Basin as part of the Overturning in the Subpolar North Atlantic Program has provided new measurements of the southward flow of Iceland-Scotland Overflow Water (ISOW) along the eastern flank of the Reykjanes Ridge. The location of the array, near 58–59°N, captures the ISOW plume at the farthest downstream location in the Iceland Basin before significant amounts of ISOW can flow into the Irminger Basin through deep fractures in the Reykjanes Ridge. The net transport of the ISOW plume at this location—approximately 5.3 Sv based on the first 4 years of observations—is significantly larger than previous values obtained farther north in the Iceland Basin, suggesting that either previous measurements did not fully capture the plume transport or that additional entrainment into the ISOW plume occurs as it approaches the southern tip of the Reykjanes Ridge. A detailed water mass analysis of the plume from continuous temperature/salinity observations shows that about 50% of the plume transport (2.6 Sv) is derived from dense waters flowing over the Nordic Sea sills into the Iceland Basin, while the remainder is made up of nearly equal parts of entrained Atlantic thermocline water and modified Labrador Sea Water. The overall results from this study suggest that the ISOW plume approximately doubles its transport through entrainment, similar to that of the Denmark Strait overflow plume in the Irminger Sea that forms the other major overflow source of North Atlantic Deep Water.

Plain Language Summary This study reports new observations of an important branch of the Atlantic Meridional Overturning Circulation known as Iceland Scotland Overflow Water. It is formed from dense Nordic Sea waters that spill across the Iceland-Scotland Ridge and mix with ambient North Atlantic waters to form a bottom-intensified current along the eastern flank of the Mid-Atlantic Ridge south of Iceland. These new observations provide the most comprehensive measurements of this flow to date—in terms of both their spatial and temporal coverage—and show that the transport of this current and the overall formation rate of Iceland Scotland Overflow Water is much larger than previously understood. The observations also indicate that approximately one-third of the Iceland Scotland Overflow Water must flow southward in the Atlantic on the eastern side of the Mid-Atlantic Ridge, rather than passing through gaps in the Mid-Atlantic Ridge to join the Deep Western Boundary Current system of the North Atlantic.

1. Introduction

Deep water formation in the North Atlantic occurs through two main processes: overflows of dense waters across the Greenland-Scotland Ridge that subsequently entrain ambient thermocline and mid-depth waters (Hansen et al., 2016; Jochumsen et al., 2015), and waters formed by intermediate depth convection in the Labrador and Irminger seas (De Jong et al., 2018; Rhein et al., 2011; Yashayaev & Loder, 2016). The North Atlantic Deep Water (NADW) formed by these processes comprises the lower limb of the Atlantic Meridional Overturning Circulation that flows southward through the Atlantic Ocean through the Deep Western Boundary Current, as well as along interior pathways (Bilo & Johns, 2019; Bower et al., 2009; McCarthy et al., 2020). The strength of the overturning circulation—and its related climatic impacts in terms of meridional heat and freshwater transport—is intimately tied to the rates of formation of NADW and to the volume of water that is added to the overflows through entrainment processes.

The overflow waters consist of two main sources, the Denmark Strait overflow between Greenland and Iceland that forms the densest component of the NADW, and the Iceland-Scotland overflow that has slightly

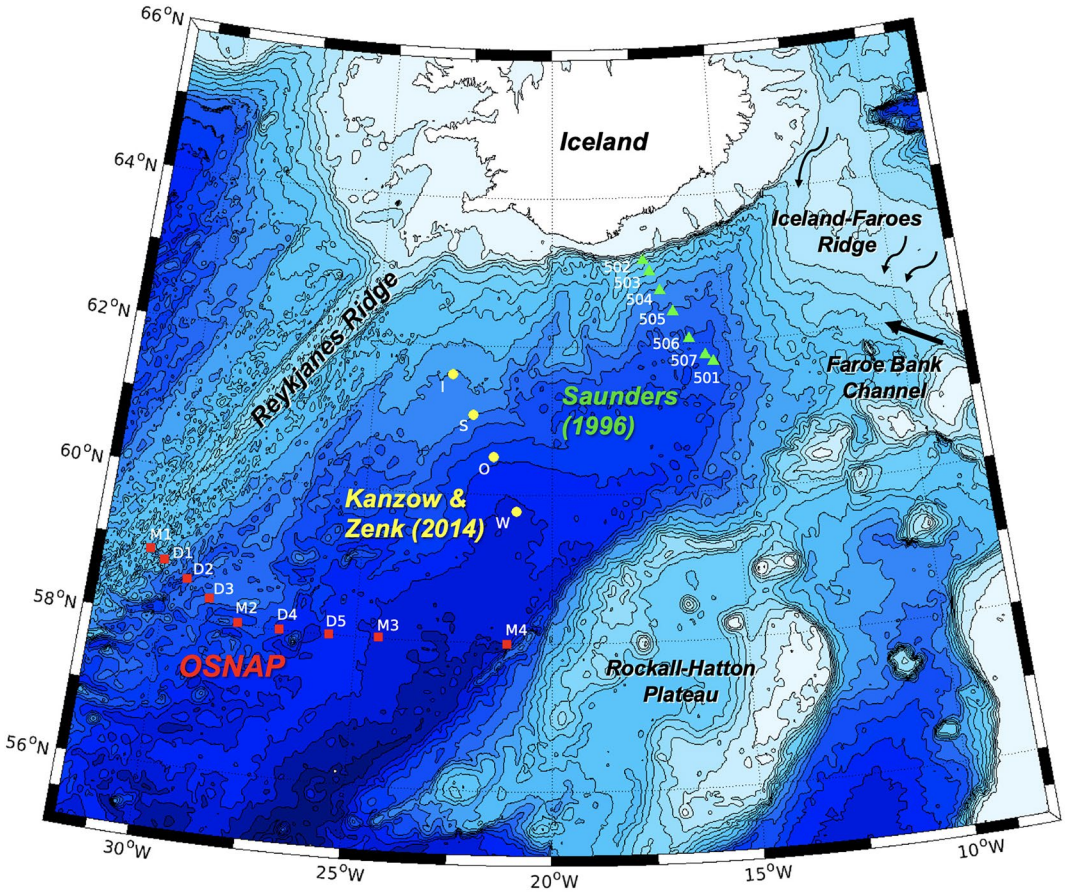

Figure 1. Map of the Iceland Basin showing the location of the Overturning in the Subpolar North Atlantic Program mooring array (in red symbols, with denoted mooring names), and the locations of two previous moored arrays (Kanzow & Zenk, 2014; Saunders, 1996) used to estimate the Iceland-Scotland Overflow Water plume transport. The location of the Faroe Bank Channel, where most of the Norwegian Sea overflow waters enter the Iceland Basin, is indicated in the upper right. Additional overflow pathways across the Iceland-Faroes Ridge are indicated by lighter arrows. Bottom topography is from the SRTM15+ Global Bathymetry (Tozer et al., 2019), that combines all available echo sounding and multi-beam data sets with satellite altimetry (updated from Smith & Sandwell, 1997).

lower density and enters the Iceland Basin mainly through the Faroe Bank Channel (FBC, Figure 1), as well as through deeper channels across the Iceland-Faroes Ridge (IFR). In the literature, these waters are typically referred to collectively as lower NADW, while the waters formed by intermediate depth convection in the Labrador and Irminger seas are typically referred to as upper NADW, or simply Labrador Sea Water.

A great deal of research has been performed over the past several decades on the processes and rates of NADW formation. The available data suggest that the deep overflows have remained relatively steady without significant long-term trends since continuous measurements of them began in the mid-1990s (Hansen et al., 2016; Jochumsen et al., 2017), while there is much greater interannual variability in the Labrador Sea Water formation rate (Kieke et al., 2007; Kieke & Yashayaev, 2015). The Denmark Strait overflow is 3.2 ± 0.6 Sv (Jochumsen et al., 2017) and approximately doubles its transport through entrainment within a few hundred kilometers downstream of the Denmark Strait sill (Dickson et al., 2008). The Iceland-Scotland overflow is less well constrained due to the broader nature of the Iceland-Scotland Ridge, but the main contribution is through the FBC which has been well studied and has a mean transport of approximately 2.0 Sv for waters denser than $\sigma_\theta = 27.8$ (Hansen & Osterhus, 2007; Hansen et al., 2016). Less is known about the overflow across the IFR, which appears to be more sporadic in nature (Hansen et al., 2018; Osterhus et al., 2008). Historical estimates have suggested a net overflow of dense waters across the IFR of O(1) Sv (Olsen et al., 2016), and Beaird et al. (2013) estimated a lower bound of the net overflow of dense waters across the IFR of 0.8 Sv from detailed glider surveys conducted along the IFR during 2006–2009. More

Table 1
Transport Estimates for the Iceland-Scotland Ridge Overflow, and for the Iceland-Scotland Overflow Water Plume in the Western Iceland Basin From Prior Mooring Arrays (Kanzow & Zenk, 2014; Saunders, 1996) and From This Study (Overturning in the Subpolar North Atlantic Program [OSNAP])

Location/Reference	Transport
Iceland-Scotland Ridge	
(a) Faroe Bank Channel (Hansen & Osterhus, 2007; Hansen et al., 2016)	2.0 ± 0.3 Sv
(b) Iceland-Faroes Ridge (Beaird et al., 2013)	≥ 0.8 Sv
63°N (Saunders, 1996)	3.2 ± 0.5 Sv
61°N (Kanzow and Zenk, 2014)	3.8 ± 0.6 Sv
58°N OSNAP (this study)	5.3 ± 0.4 Sv

recently, Hansen et al. (2018) suggested that the total IFR overflow may be less, based on new current meter observations showing a weak overflow through the "Western Valley" just east of Iceland, which had previously been thought to be one of the major inflow channels through the IFR.

The waters comprising the Iceland-Scotland overflow include Norwegian Sea Deep Water (NSDW) and Norwegian Sea Arctic Intermediate Water (NSAIW) that are formed by deep and intermediate convection in the Norwegian Sea, as well as a less dense component formed northeast of Iceland known as Modified East Icelandic Water (MEIW) (Beaird et al., 2013; Hansen & Østerhus, 2000). Historically the overflow waters contributing to the Iceland-Scotland Overflow Water plume (hereafter ISOW plume) have been considered as those with densities greater than $\sigma_\theta = 27.8$, which include the above three water types. The largest fractions of NSDW and NSAIW (often referred to collectively as Norwegian Sea Overflow Water, NSOW) flow through the FBC, with smaller amounts also sporadically flowing across the IFR (Hansen & Østerhus, 2000). While some MEIW flows through the FBC overlying the denser NSOW components, the bulk of the MEIW overflow is believed to occur across the IFR, and is probably the least constrained contribution to the total overflow (Beaird et al., 2013).

A puzzling aspect of the ISOW plume's development in the Iceland Basin is the apparently low rate of entrainment into the overflow, compared to the approximate transport doubling known to occur for the Denmark Strait overflow. Previous observations based on moored arrays across the ISOW plume (Table 1) have found transports that are only slightly larger than the ~3 Sv of overflow waters crossing the Iceland-Scotland Ridge. For example, Saunders (1996) found an ISOW plume transport of 3.2 Sv from an array deployed just south of Iceland, and Kanzow and Zenk (2014) found a transport of 3.8 Sv farther downstream near 61°N (see Figure 1), of which approximately 0.4 Sv was found to recirculate northward in the Iceland Basin.

Nevertheless, there is clear evidence for entrainment of lighter waters into the ISOW plume based on observed changes in its water mass properties downstream from the sills. Within a few hundred kilometers downstream of the IFR, the densest waters in the ISOW plume have potential temperatures and salinities of approximately 2.5°C and 34.97 (Saunders, 1996), substantially warmer and saltier than the NSOW flowing through FBC with potential temperatures from −1.0 to 0.5°C and salinities near 34.90. This rapid increase in the temperature and salinity of the ISOW plume indicates substantial mixing with warm and salty Atlantic thermocline waters ($\theta = 7$–8°C, $S = 35.20$) that overlie the NSOW where it exits from the FBC (Hansen & Østerhus, 2000; Van Aken & De Boer, 1995). Further dilution of the plume occurs through mixing with modified Labrador Sea Water that occupies the subthermocline layer in the Iceland Basin. Saunders (1996) concluded that entrainment of these two source waters into the ISOW plume resulted in a ~50% dilution of the original NSOW, leading to an estimate of only 1.6 Sv of NSOW being contained within the plume, smaller than the ~2.0 Sv of NSOW known to be overflowing through the FBC (Hansen et al., 2016). Also, Saunders at that time did not consider any possible contribution of MEIW to the total overflow. This led Hansen et al. (2016) to conclude that Saunders's observations had likely underestimated the strength of the plume or may have possibly missed some portion of it. Other estimates from single hydrographic cruises have estimated ISOW plume transports as high as 5–6 Sv (Dietrich, 1956; Steele et al., 1962), but the majority of estimates (summarized by Kanzow & Zenk, 2014) put the plume transport at between 3 and 4 Sv all along the Reykjanes Ridge from Iceland to 58°N. Similar estimates were found from the OVIDE program (Daniault et al., 2016; García-Ibáñez et al., 2018) that

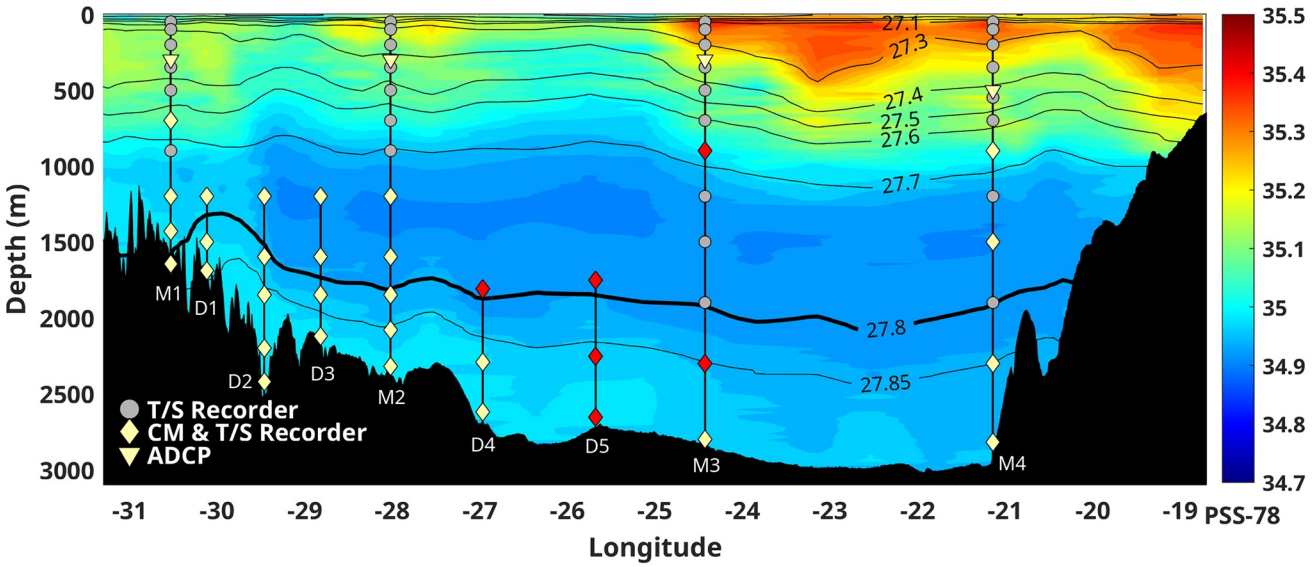

Figure 2. Overturning in the Subpolar North Atlantic Program mooring array configuration overlaid on a shipboard CTD salinity section across the Iceland Basin during July 2014. The section runs from the crest of the Reykjanes Ridge on the left to the Rockall-Hatton Plateau on the right. High salinities are found in the near-surface layer on the eastern side of the section associated with the North Atlantic Current; low salinities at intermediate depths associated with Labrador Sea Water, and higher salinities near the bottom along the eastern flank of the Reykjanes Ridge associated with the Iceland-Scotland Overflow Water (ISOW) plume. The $\sigma_\theta = 27.8$ isopycnal, denoting the ISOW layer, is indicated in bold. The originally deployed array in July 2014 is denoted by yellow and gray symbols; instruments marked in red were added in July 2016.

crossed the ISOW plume near 58°N, close to the location of the new observations we describe in this study. García-Ibáñez et al. (2018) reported a mean ISOW plume transport of 3.2 ± 0.4 Sv from six OVIDE cruises occupied between 2002 and 2012, but a higher estimate of 5.1 Sv from the OVIDE cruise in 2014.

In this study, we report on the results from the first 4 years of a mooring array deployed across the ISOW plume near 58°N, as part of the Overturning in the Subpolar North Atlantic Program (OSNAP; Lozier et al., 2019). This is the most comprehensive moored array across the ISOW plume to date, involving a larger number of current meters deployed within the plume than in earlier studies (Kanzow & Zenk, 2014; Saunders, 1996), and with roughly twice (or longer) the temporal duration of these earlier studies. The array also includes direct temperature/salinity measurements paired with each current meter in the array, to provide continuous estimates of the water mass composition of the plume. Our results show a larger mean plume transport (5.3 ± 0.4 Sv) than found in most previous studies, and we show through water mass analysis that the amount of original overflow source waters contained in the plume is consistent with the amount of overflow waters coming over the sills, within uncertainties. The results suggest that the ISOW plume does in fact approximately double its transport through entrainment, similar to the behavior of the Denmark Strait overflow plume, which represents an important change in the understanding of the net production and export of ISOW from the Iceland Basin.

2. Data and Methods

2.1. Moored Current Meters and Temperature/Salinity Recorders

As part of OSNAP, a set of nine taut-wire subsurface moorings were set across the Iceland Basin between the crest of the Reykjanes Ridge and the western edge of the Rockall-Hatton Plateau (Figure 1). The array was designed to capture several key elements of the eastern subpolar gyre circulation: (a) the Deep Western Boundary Current (DWBC) along the eastern flank of the Reykjanes Ridge, composed of ISOW and its entrainment products; (b) the northward flow of upper ocean waters transported by the main branches of the North Atlantic Current toward the Nordic Seas; and (c) the southward recirculation of the broader cyclonic subpolar gyre along the Reykjanes Ridge's eastern flank within the East Reykjanes Ridge Current (ERRC; Koman et al., 2020). The tall moorings M1–M4 (Figure 2) were configured as "dynamic height" moorings with vertical arrays of temperature/salinity recorders (Seabird 37-SM microcats) spaced through

the water column that allow estimates of the relative geostrophic transport over the broad areas between them. Each of the tall moorings M1–M4 also had upward-looking Acoustic Doppler Current Profilers (ADCPs) at depths between 300 and 500 m to observe the near-surface currents at those locations. Over the eastern flank of the Reykjanes Ridge, a denser set of short moorings (D1–D5) was deployed to monitor the ISOW plume at depths below 1,200 m. These moorings had paired current meters and T/S recorders at 3–5 depths between 1,200 m and the bottom, and together with similar instrumentation on the deep parts of M1 and M2, provide measurements across the full extent of the ISOW plume from the crest of the Reykjanes Ridge to the central Iceland Basin. Details of the instrument sampling configurations and the processing and quality control of the data are contained in the Supporting Information.

The array was first deployed in July 2014 and was subsequently serviced in June 2015, July 2016, and July 2018. The data presented in this study therefore span a period of 4 years from July 2014 to July 2018, resulting in a 1460-day common time period for all data records. Individual moorings in the array were typically recovered and redeployed on the same day (or on the following day), resulting in only small gaps in the time series records that were filled by linear interpolation. The originally deployed array consisted of the eight moorings M1, D1, D2, D3, M2, D4, M3, and M4 (from west to east across the Iceland Basin), and that configuration was maintained for the first 2 years of observations from July 2014 to July 2016 (Figure 2). In July 2016, an additional mooring (D5) was added between moorings D4 and M3 to better capture the deeper reaches of the ISOW plume, and instrumentation was enhanced on two moorings (an upward extension of mooring D4 to 1,800 m and two additional current meters on mooring M3), as shown in Figure 2.

For the purposes of this study, all time series records have been low-pass filtered using a fourth order Butterworth filter with a 40-h cutoff period to eliminate tides and fluctuations associated with internal/inertial waves.

2.2. Argo and Altimetry Data

Most of the analysis presented in this study is based on the above moored time series data. However, we also use Argo float data and satellite altimetry data to help constrain the deep transports within the ISOW layer in the eastern part of the Iceland Basin where the mooring data is sparse. Specifically, we use both surface velocities derived from altimetry and 1,000 m drift data from Argo floats to reference the geostrophic transports between the broadly spaced dynamic height moorings M2, M3, and M4 (Figure 2).

Estimates of surface geostrophic velocity from the 1/4° Aviso+ blended altimetry analysis were obtained from the Copernicus Marine Environmental Monitoring Service (CMEMS) for the period from 1992 to 2018. The available Argo 1,000 m drift data from 1997 to 2018 was obtained from the Asia-Pacific Data-Research Center (APDRC) and similarly averaged onto a 1/4° grid using the methodology described in Bilo and Johns (2019). The Argo drift analysis of Bilo and Johns (2019) is publicly available at https://doi.org/10.17604/cf5z-x124.

2.3. Shipboard CTD and Lowered-ADCP Data

During the mooring deployment and recovery cruises in the summers of 2014, 2015, and 2016, CTD and lowered-ADCP (LADCP) sections were acquired across the western portion of the array from the Reykjanes Ridge crest to the location of mooring D5. The CTD/LADCP stations were spaced 12–16 km apart with highest resolution along the upper ridge crest. The LADCP data were processed using version IX_13 of the LDEO LADCP processing software maintained by M. Visbeck and A. Thurnherr (https://www.ldeo.columbia.edu/~ant/LADCP/), including the use of on-station vessel-mounted ADCP (VM-ADCP) data and bottom-track data from the LADCP to constrain the final velocity profiles.

Geostrophic velocity profiles were produced for each pair of stations and referenced to the spatially averaged VM-ADCP data acquired between the station pairs, over the range of good upper-ocean data provided by the ADCPs (typically to 600–800 m using 75 kHz VM-ADCP systems). On the 2016 cruise, the VM-ADCP data were of poor quality and only LADCP velocity profiles were available (with no upper-ocean VM-ADCP constraint). The resulting LADCP and geostrophic velocity sections have about 2–3 times the spatial

resolution of the moorings and are used to check the transports derived from the moored array during the time periods when the shipboard sections were acquired.

2.4. Gridding of the Mooring Data and Estimation of ISOW Transport

As we will show in the Results section, the southwestward flow of the ISOW plume is confined to the region between moorings M1 and D5 along the eastern Reykjanes Ridge flank. To estimate the transport of the ISOW plume, the current meter data at each site is first fit to a shape-preserving cubic spline in the vertical using the "pchip" Piecewise Cubic Hermite Interpolating Polynomial routine in Matlab (Gupta, 1991), and saved at 50 m vertical resolution with extension of the deepest measurement level to the bottom. The resulting current profiles are similar to those produced by Akima spline interpolation (Akima, 1970), passing exactly through the measured data points at the current meter levels but without permitting any extrema to be created between data points. Following this, a two-dimensional "natural neighbor" interpolation (Sibson, 1981; Watson, 1992) is performed across the full array from moorings M1–D5 and sampled on a 10 m vertical by 2 km horizontal grid. The resulting gridded current field is similar to that produced by a simple linear two-dimensional (triangular) interpolation except that it produces slightly smoother fields without abrupt transitions in velocity gradients at the mooring locations. As in linear interpolation, the fields agree exactly with the original data at the measurement locations. Tests using both linear and natural neighbor interpolation showed only minor differences in computed transports, typically less than 0.1 Sv for daily estimates and within 0.02 Sv for the time mean transport, which is negligible compared with the statistical uncertainty of ±0.3 Sv for the ISOW plume mean transport (to be discussed further in Results). The gridded current fields were produced at daily intervals, based on the 40-h lowpass filtered data records. The exact same gridding procedure was applied to the temperature and salinity records from the moorings, and the corresponding potential density fields. The transports for the ISOW plume are estimated by summing all flow contributions below the $\sigma_\theta = 27.8$ interface, which also varies in its location on a daily basis.

To account for the missing data at mooring D5 during the first 2 years (2014–2016), the time mean flow profile at mooring D5 from the last 2 years (2016–2018) was substituted for all times during the first 2 years in the above two-dimensional interpolation procedure. This results in a somewhat reduced variability of the total plume transport during the first 2 years, but should not lead to a significant bias in the mean transport for that period. (Note that the mean currents at all other sites were remarkably consistent between the first 2 years and last 2 years of the record, and even for individual annual averages, lending support to this statement). In addition, a method had to be found to fill in the top measurement level (at 1,820 m) on mooring D4 during the first 2 years, since the 1,820 m sensor was only added to the array in 2016 (Figure 2). From the 2016–2018 data on mooring D4, a robust linear relationship was found between the currents at the 1,820 m and 2,320 m levels ($r = 0.7$ for the 215°T alongslope component; °T = relative to true north), with the 1,820 m currents having about 60% of the variability observed at the 2,320 m level, and this linear relationship was used to fill the 1,820 m level. For temperature and salinity, a multiple regression was used to fill the 1,820 m T/S records based on the nearby records from M2 (at 1,600 m and 1,860 m; see Figure 2) and the 2,320 m level on D4, which gave a good approximation of the T/S records at the 1,820 m level on mooring D4 during 2016–2018, with no bias.

Prior to computing transports, a 30-m thick bottom boundary layer was added to the gridded velocity data, by linearly reducing the velocity at 30 m off the bottom to zero at the bottom across the entire array. The choice of 30 m for the bottom boundary layer is somewhat arbitrary but is consistent with the average thickness of the bottom boundary layer found in previous studies of the ISOW and Denmark Strait Overflow Water (DSOW) plumes (Beaird et al., 2013; Jochumsen et al., 2017) as well as in other dense water plumes such as the Mediterranean and Red Sea outflow plumes (Baringer & Price, 1997; Peters et al., 2005). Application of this bottom boundary layer correction results in a reduction of the total plume transport by 0.15 Sv compared to the calculation without it being applied. We also note that the topography along the mooring line—measured precisely by multi-beam echo sounding during the initial deployment cruise—is slightly modified for transport estimation purposes, with certain areas being filled in that are associated with localized topographic depressions that have a short (<50 km) alongstream scale, and in which no current meter data was directly available. These areas are indicated by the gray shading in Figure 6a (see Section 3), and

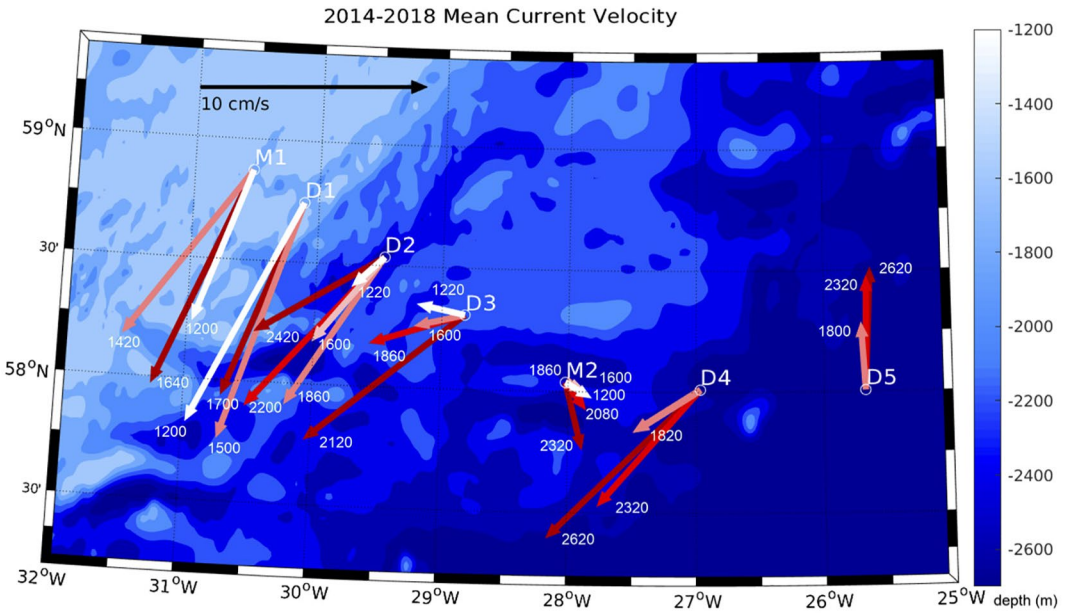

Figure 3. Four-year mean currents at depths ≥1,200 m across the Iceland-Scotland Overflow Water plume, from mooring sites M1 to D5. White vectors show the mean currents at 1,200 m; darker colors show the currents at increasing depth to within 50 m above the bottom.

the tops of these gray areas, or the actual topography otherwise, represent the effective topography across the array for the purposes of computing transport.

3. Results

3.1. Mean Flow and Variability of the ISOW Plume

The 4-year mean currents recorded on moorings M1–D5, which span the ISOW plume along the Reykjanes Ridge's eastern slope, are displayed in Figure 3. The currents are aligned generally along the Ridge topography and perpendicular to the mooring line with maximum mean speeds of approximately 0.1 m/s near the bottom. At moorings M1 and D1, on the upper Reykjanes Ridge (RR) slope, the currents tend to be more vertically uniform up to the top of the ISOW plume array (at 1,200 m depth), whereas at the other sites the flow is bottom intensified and shows relatively weak mean flow at 1,200 m (e.g., at moorings D2, D3, and M2).

A notable feature of the mean flow distribution is the much weaker mean flow observed at mooring M2, and the again strongly bottom-intensified southwestward flow at mooring D4. Farther eastward, at mooring D5, the flow is northward and also shows a bottom-intensified structure, indicating a possible recirculation of ISOW plume waters to the east of the main plume. The relative minimum in the plume speeds near mooring M2 appears to be due to a bifurcation of the ISOW plume into two branches upstream of the OSNAP array: one that follows the upper RR slope, and a secondary branch that follows the deeper topography along the lower RR slope and passes through mooring D4. This interpretation is supported by modeling studies that also show such a bifurcation of the ISOW plume occurring near 59–60°N (Xu et al., 2010; Zou et al., 2017), related to a local promontory in the RR slope topography that causes an offshore diversion of the deeper part of the ISOW plume around this feature to the southeast before again following the deeper RR isobaths toward the southwest. To illustrate this, Figure 4 shows a comparison of the deep currents observed at the OSNAP array with the deep currents derived from the 1/12° FLAME model analyzed by Zou et al. (2017), where a deeper branch of the ISOW plume can clearly be seen splitting off from the main plume near 60°N to follow a pathway through the location of mooring D4. The model also suggests that there can be multiple branches of the ISOW plume at other locations, for example along the broader topographic slope south of Iceland near 23–24°W where the model shows three distinct plume branches, with the deepest of these

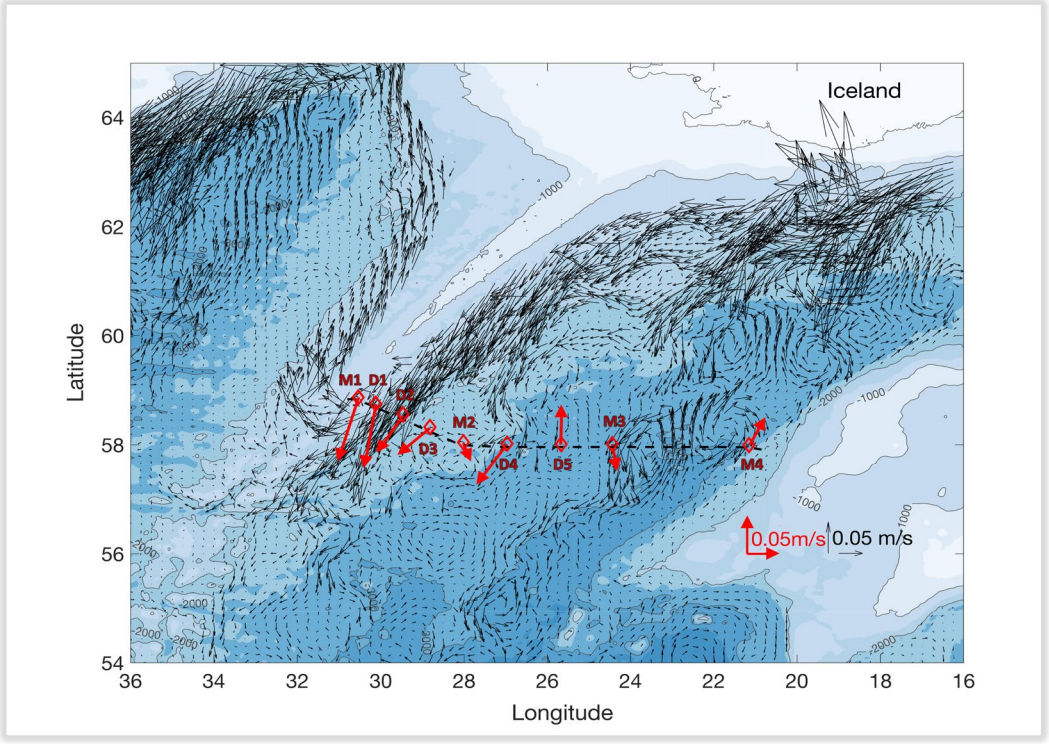

Figure 4. Fifteen-year mean currents from the FLAME model, with Overturning in the Subpolar North Atlantic Program 4-year mean currents overlaid (in red), averaged over the density layer $\sigma_\theta > 27.8$.

three branches also possibly feeding partly into the deep plume branch on the OSNAP line at mooring D4. Details of the FLAME model configuration are described in Zou et al. (2017).

There are some aspects of the FLAME model results that are not consistent with the observations, for example, the strong northward recirculating flow at D5 is not represented in the model, and the ISOW plume flow at D3 is underestimated in the model, perhaps indicating a greater impact of the above-described topographic feature in blocking the plume's flow in the model than occurs in reality. Figure 4 also shows the deep currents observed at moorings M3 and M4 in the eastern Iceland Basin, where the mean flow is southward at M3, and then northward again at M4, indicating an alternating pattern of the deep flow across the central and eastern Iceland Basin, although one that is likely poorly resolved by the sparse mooring observations. The model suggests that the southward flow observed at mooring M3 is related to a local recirculating feature rather than having any direct connection to the ISOW plume farther north in the basin.

The variability of the deep currents across the array is illustrated in Figure 5 by vector time series plots from the deepest current meter level on each mooring, which were typically placed at 50 m above the bottom, except at mooring D2 which was located in a local topographic depression and for which the bottom current meter was placed at 100 m off the bottom. Along the upper RR slope from moorings M1 to D3, the flow is persistently southwestward, with few reversals, and a similarly persistent southwestward flow occurs at mooring D4. Maximum speeds in the upper plume reach up to ~0.3 m/s at M1, with slightly weaker values of 0.2–0.25 m/s farther down the slope as well as at D4. The flow at mooring M2 is also persistently southward but with smaller maximum speeds of ~0.15 m/s, and with few exceptions, it is consistently weaker than the neighboring flows at D3 and D4.

The deep flow at mooring D5 (only available for 2016–2018) is also persistently northward with only occasional reversals, while those at M3 and M4 are more variable. The near-bottom flow at M4 is closely aligned with the topographic orientation of the deep Rockall-Hatton Bank slope, with a preponderance of strong northeastward flow events. Maximum flows at these sites can reach similar magnitudes to those observed in the ISOW plume, of ~0.3 m/s. Owing to the 4-year length of the records, which have calculated integral

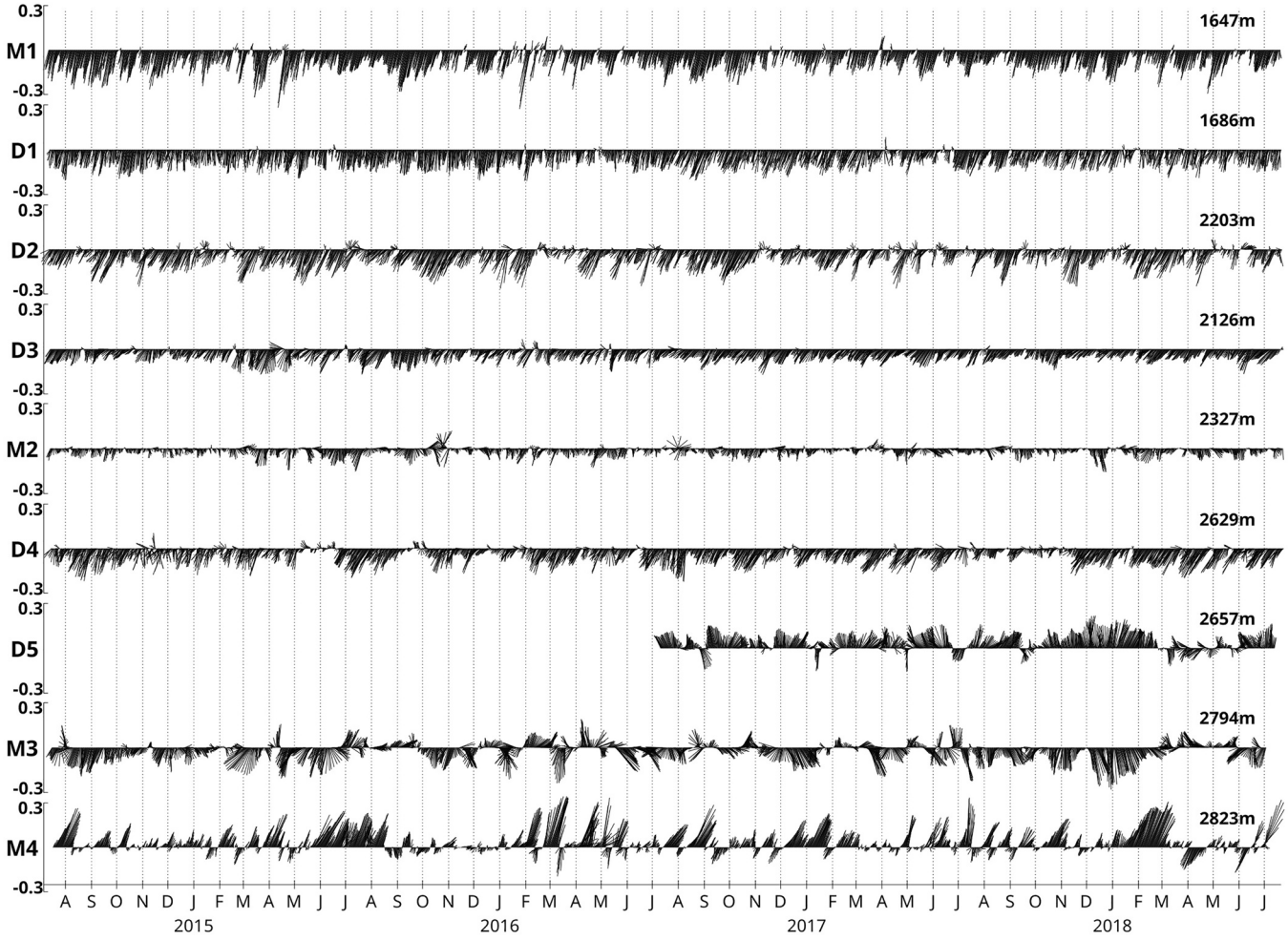

Figure 5. Four-year time series of near-bottom currents at all mooring sites across the Iceland Basin. Depths of measurement are indicated at the right. North is up; velocities are in m/s.

time scales of typically 10–20 days, and therefore approximately 40–80 degrees of freedom, nearly all of the measured mean currents are significantly different from zero (Table S1 contains the mean flows, standard deviations, and standard errors for all of the current meters below 1,200 m across the array).

A cross-section of the mean flow observed by the array, rotated into the mean alongstream direction of the ISOW plume (215°T), is shown in Figure 6a from the top of the RR to mooring D5. The separation of the plume into a branch along the upper RR slope, from moorings M1–D3, and a lower branch centered near D4, is clearly evident. The flow is bottom intensified eastward of mooring D1—hugging the bottom as is to be expected for the ISOW plume—with weak flow at M2 and then the secondary bottom intensified offshore branch at D4. However, on the upper ridge crest the plume merges into the lower part of the ERRC, which has a nearly barotropic structure (Koman et al., 2020) and extends quasi-uniformly to the surface above the 1,200 m level. Therefore, it is not straightforward to determine where the flow associated with the ISOW plume "ends" and the flow associated with the ERRC begins. Nevertheless, if the traditional definition of the ISOW layer is used, with ISOW being defined as waters with potential densities of $\sigma_\theta > 27.8$ (Hansen & Østerhus, 2000), then the lower part of the ERRC clearly contains waters that are part of the ISOW layer (note the $\sigma_\theta = 27.8$ contour drawn in Figure 6a). For the purposes of this paper, we will continue to use the classical definition of ISOW in the Iceland Basin (i.e., $\sigma_\theta > 27.8$), and all transports computed for the ISOW plume will include waters with potential density $\sigma_\theta > 27.8$.

Figures 6b and 6c show the mean distributions of potential temperature and salinity across the array, derived from the moored T/S recorders deployed on the moorings, with σ_θ contours overlain on each panel for

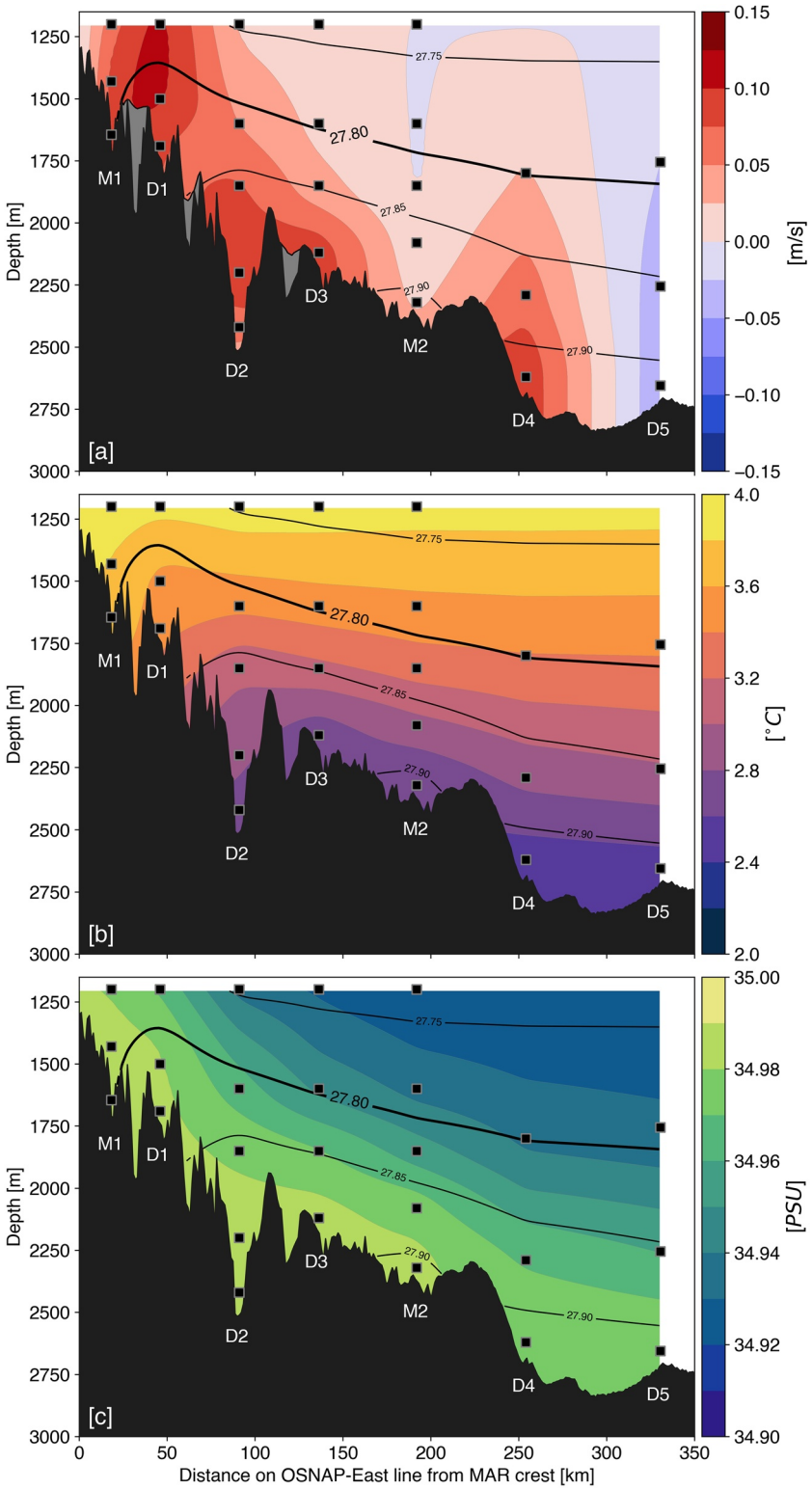

Figure 6. Mean (a) along-ridge velocity (cm/s), (b) potential temperature (°C), and (c) salinity (psu) derived from the Iceland-Scotland Overflow Water plume mooring array. Symbols show the locations of current meters and collocated T/S recorders. Black contours show the location of σ_θ surfaces; the mean location of the $\sigma_\theta = 27.8$ contour is shown in bold. Gray shaded areas in (a) show localized topographic depressions that are filled in for transport computation purposes.

reference. A notable feature of the potential density field is the downward deflection of density surfaces into the steep topography along the upper ridge crest, a signature that is suggestive of intensified near-bottom mixing (Callies & Ferrari, 2018; St. Laurent et al., 2001). This feature is linked primarily to the temperature field, which shows potential temperature isopleths bowing downward near the bottom as far offshore as M2, while the salinity field shows a nearly uniform layer of characteristically higher salinities along the bottom associated with ISOW, with salinities reaching 34.98 near the bottom.

3.2. Transport of the ISOW Plume

Using the methodology described in Section 2.4, daily estimates of the ISOW plume transport were produced for the period from July 15, 2014 to July 13, 2018, a total length of 1,460 days. The time mean transports computed for different regions of the plume ($\sigma_\theta > 27.8$) are as follows:

1. -4.53 ± 0.22 Sv for the "upper" plume branch from the crest of the RR to mooring M2.
2. -1.61 ± 0.26 Sv for the "lower" plume branch from mooring M2 to the location of the time-mean zero-crossing of the flow between moorings D4 and D5 (at ~300 km on Figure 6a).
3. -0.78 ± 0.34 Sv for the net transport computed from mooring M2 all the way to mooring D5. The above uncertainties represent standard errors based on the observed autocorrelation time scales of the transport time series (ranging between 7 and 10 days), computed in the same manner as described earlier for the mean currents.

Integrating the transports over the above regions (1) and (2) together yields a total plume transport of -6.14 ± 0.31 Sv, while integrating over regions (1) and (3) together yields a mean transport of -5.31 ± 0.35 Sv. The first value (-6.14 Sv) can be taken as an estimate of the actual southward plume transport along the eastern flank of the RR, but it could be an overestimate of the net export of ISOW from the Iceland Basin due to the observed northward recirculation at mooring D5, which has virtually identical T/S properties to the water at mooring D4 (as will be shown later). Unfortunately, the current meter data to the east of mooring D5 is too sparse to resolve the width of the northward recirculation at D5, or to compute direct transports for the rest of the basin.

Therefore, to estimate the net transport of ISOW across the eastern part of the section, including any recirculating component, we use the dynamic height moorings M2, M3, and M4 to make an independent estimate of the spatially integrated transport over the distances between them. For each mooring, the temperature and salinity profiles from the moored CTD sensors are first interpolated in the vertical using the "pchip" shape-preserving cubic spline, and dynamic height profiles are created at each site. The time-mean geostrophic velocity profile between each pair of moorings is then calculated and referenced to two estimates of absolute velocity: (a) the spatially integrated surface velocity between each mooring pair derived from the Aviso+ altimetry analysis, and (b) the spatially integrated Argo drift velocity at 1,000 m between each mooring pair from the Bilo and Johns (2019) analysis. The time mean values of these reference velocities are taken over the full data periods available for each data set (1992–2018 for altimetry; 1997–2018 for Argo) to obtain the most representative estimates.

To capture the geostrophic shear associated with the lower branch of the ISOW plume at D4, the dynamic height profile at M2 is extended vertically by appending the deepest CTD sensor on mooring D4 (at 2,630 m) to the M2 T/S profiles. This is consistent with best practices in applying "endpoint" geostrophic techniques (Ganachaud, 2003; McCarthy et al., 2015) and should provide a close approximation of the net geostrophic flow between moorings M2 and M3 to the extended depth of M2 (2,630 m). The corresponding geostrophic velocity profile for the M3-M4 mooring pair extends to a depth of 2,800 m. These geostrophic velocity profiles are then linearly extrapolated to the bottom and masked by the bottom topography to obtain transport profiles for the regions between M2-M3 and M3-M4. The results of this calculation are shown in Figure 7, where the corresponding transports for the layer below $\sigma_\theta = 27.8$ are obtained by integrating these profiles vertically below mean depth of the $\sigma_\theta = 27.8$ isopycnal for each mooring pair.

For the M2-M3 mooring pair, the results using the two different reference velocity estimates agree relatively closely, with both indicating southward flow beginning at 1,800–2,000 m and with transport estimates for $\sigma_\theta > 27.8$ of -1.8 Sv and -1.4 Sv for altimetry and Argo reference, respectively. For the M3–M4 pair, the results show greater disagreement (1.0 Sv for altimetry reference and 0.4 Sv for Argo reference), but in both

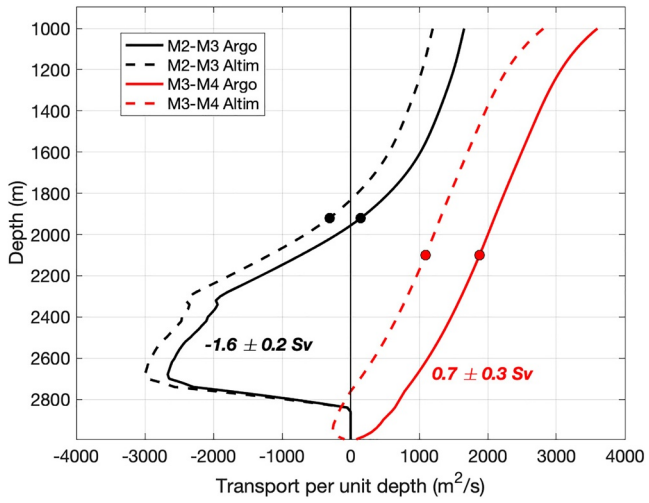

Figure 7. Mean transport-per-unit-depth profiles below 1,000 m between moorings M2–M3 (black) and M3–M4 (red), derived from time-mean dynamic height profiles at the moorings referenced to climatological Argo (YoMaHa) 1,000 m drift data across the eastern Iceland Basin (solid curves) and to surface geostrophic velocity from altimetry (dashed curves). The mean depth of the $\sigma_\theta = 27.8$ isopycnal for each mooring pair is shown by colored dots. The transport values listed represent the average of the two estimates below $\sigma_\theta = 27.8$ (−1.6 Sv for M2–M3, and 0.7 Sv for M3–M4), and their respective uncertainties.

cases show a net northward flow in the deep $\sigma_\theta > 27.8$ layer. For the final estimates of these geostrophic transports, we take the average of the two estimates for each mooring pair (−1.6 ± 0.2 Sv for M2–M3; 0.7 ± 0.3 Sv for M3–M4), with uncertainties reflecting the difference between the two estimates. Thus, for the central and eastern portion of the basin between moorings M2 and M4, the estimated transport for the $\sigma_\theta > 27.8$ layer from these geostrophic calculations is −0.9 ± 0.4 Sv (southward), net of recirculation.

The flow in the bottom triangle east of M4 (see Figure 2) is neglected in this estimate, and the bottom intensified northward flow observed at M4 could lead to a northward transport in that region of up to 0.2 Sv if uniformly extended to the boundary, but is likely to be smaller.

The above estimate, of −0.9 Sv for the entire ISOW layer between moorings M2 and M4, is nearly the same as the estimated transport of −0.78 Sv that is derived from the direct current meter observations for the region between M2 and D5. This suggests that the current meter derived transport for the western region between M2 and D5—inclusive of the part of the recirculation near D5 that is captured within this area—is representative of the net southward ISOW transport all across the basin between M2 and the Rockall-Hatton Bank. Therefore, we will use the directly computed moored transport over the region from moorings M1 to D5 as our best estimate of the southward transport of the ISOW plume, including any net recirculation across the rest of the basin.

3.3. Variability of the ISOW Plume Transport

Daily transport estimates over the total plume domain from moorings M1–D5 show a wide range of variability from >15 Sv southward to 5 Sv northward, while for 30-day lowpass filtered values the transports typically range from 0 to 10 Sv southward (Figure 8a). The upper branch of the plume, from M1 to M2, shows a weaker variability (Figure 8b), with daily values ranging from about 0–10 Sv to about 2–8 Sv for 30-day lowpass filtered data, even though it

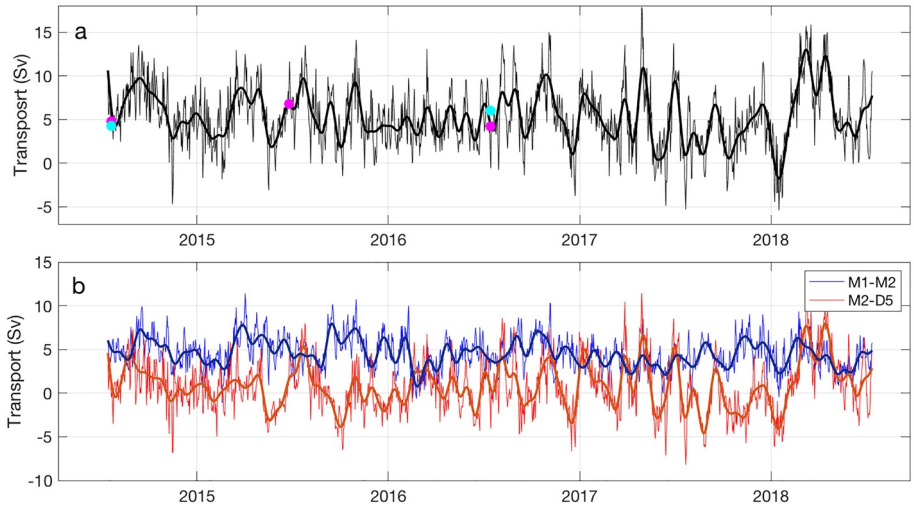

Figure 8. Transport time series of the Iceland-Scotland Overflow Water plume: (a) total transport, (b) transport contributions of the upper (M1–M2) and lower (M2–D5) plume branches. Thin lines are daily average values; thick lines are 30-day lowpass filtered values. Cyan and magenta dots in (a) show the corresponding plume transports derived from CTD sections (referenced to vessel-mounted Acoustic Doppler Current Profiler [ADCP]), and from lowered-ADCP sections across the plume, respectively.

accounts for 85% of the time mean plume transport (4.5 Sv of the total 5.3 Sv). Most of the extremes of the total transport are related to the variability of the transport in the lower plume domain, which actually has a higher variance (standard deviation of 3.0 vs. 1.9 Sv for the upper plume), with daily values ranging from >10 Sv southward to >5 Sv northward.

The transports of the upper and lower plume regions are statistically uncorrelated ($r = -0.02$), and therefore their variances nearly add up (within 1%) to the variance of the total plume transport, which has a standard deviation of 3.5 Sv. At certain times, the two transport time series do show some degree of covariation, such as during January 2018 when the upper plume transport was near its minimum strength and the lower plume transport was strongly northward, leading to an extreme (northward) transport event across the entire array. However, overall there is no observed tendency for the transports within the upper and lower plume branches to either compensate or covary with each other.

Temporal variations of the total plume transport occur over a broad range of time scales, with no particular dominant period of variation. The power spectra of the ISOW plume transport for the total transport (not shown), and for the two branches separately, are red and relatively featureless, with a minor peak near 100 days that is mostly associated with the transport variability in the lower plume domain. We believe the higher transport variability in the lower plume domain is due in part to the effects of deep-reaching mesoscale eddies that are prevalent in the central Iceland Basin, linked to the variability of the North Atlantic Current that exhibits a surface eddy kinetic energy (EKE) maximum near the location of mooring M3, and that extends westward to the locations of moorings D5 and D4 with still elevated EKE values (Zhao et al., 2018). Over the upper plume region, where the surface EKE values are substantially lower, the effects of these eddies should be correspondingly less, and the observed transport variations appear to be more intrinsic to the plume variability itself. While a detailed analysis of the plume variability will be the subject of a future study, we show in the Supporting Information (Figure S1) a few snapshots of the plume structure observed during periods of extreme high and low transports, and for a typical state with a transport close to its mean value. In the extreme transport cases, the flow in the D4/D5 region shows northward (southward) anomalies over much of the deep-water column in the high (low) transport cases that appear to be superimposed on the lower plume velocity core near mooring D4 and primarily cause the extreme transports at these times.

The transports computed from the mooring array were checked against the corresponding transports derived from the CTD and LADCP sections available during the mooring servicing cruises, as described in Section 2.3. These transports are plotted in Figure 8a on top of the mooring-derived transport time series, and in each case agree with the mooring-derived estimate within ±1 standard deviation of the time-mean moored transport over the period of time it took for the sections to be completed. Some of the CTD/LADCP sections were more synoptic than others: the first section in 2014 was done after the mooring array was fully deployed and took only 3 days to complete, while during 2015 and 2016 the sections were interspersed with mooring operations and took 5 and 7 days to complete, respectively. The largest discrepancy occurred during 2016 when the CTD and LADCP derived transports were different by 1.8 Sv (4.2 Sv for the LADCP section, and 6.0 Sv for the CTD section), with the moored transport estimate of 3.9 ± 2.7 Sv agreeing more closely with the LADCP transport, but still within the range of the CTD transport. These comparisons, although limited, give us confidence that the mooring array is adequately resolving the ISOW plume structure and producing accurate, unbiased transport estimates.

3.4. Water Mass Composition of the ISOW Plume

Given the larger transport estimate for the ISOW plume we find in this study compared to those from previous studies farther north in the Iceland Basin (Kanzow & Zenk, 2014; Saunders, 1996), a logical question to ask is: Can the observed transport be rationalized against the known transport of dense overflow waters crossing the IFR, after accounting for the entrainment of lighter waters into the overflow? To answer this question, we perform a water mass analysis of the ISOW plume to determine the volume-flux weighed contribution of different source waters to the plume, including the original overflow source waters (NSOW and MEIW) and the primary waters entrained into the plume (Atlantic thermocline water, commonly referred to as Subpolar Mode Water [SPMW], and Labrador Sea Water [LSW]).

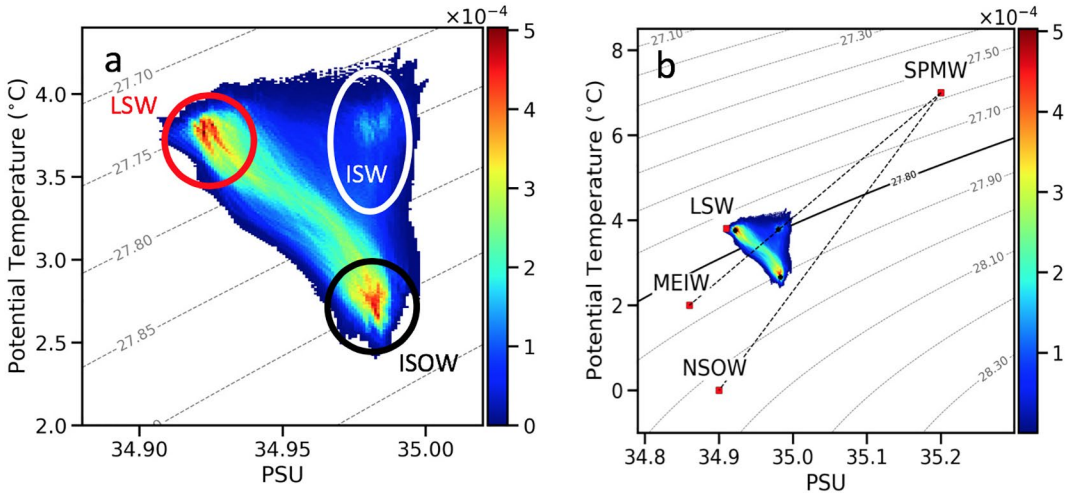

Figure 9. Water mass composition of the ISOW plume: (a) mean θ/S frequency distribution of gridded θ/S data below 1,200 m from moorings M1–D5, (b) as in (a) but expanded to show water mass mixing endpoints (SPMW = Subpolar Mode Water, LSW = Labrador Sea Water, MEIW = Modified East Icelandic Water, NSOW = Norwegian Sea Overflow water). The circled areas in (a) show the main water mass cores found within the plume (LSW = Labrador Sea Water, ISOW = Iceland-Scotland Overflow Water, ISW = Icelandic Slope Water).

To begin, we show in Figure 9a the water mass properties of the ISOW plume in the form of a potential temperature/salinity (θ/S) frequency distribution derived from the gridded arrays of θ and S below 1,200 m across the array from moorings M1 to D5. The highest concentration of θ/S values occur in two cores, one at [2.6–2.7°C, 34.98] corresponding to the core properties of ISOW, and the other at [3.8–3.9°C, 34.92] corresponding closely to the properties of LSW that overlie the ISOW layer within the Iceland Basin. A third, weaker core occurs near [3.8°C, 34.98] that corresponds to the properties of so-called "Icelandic Slope Water" (ISW) that has been identified in prior hydrographic studies along the RR slope south of Iceland (Read, 2000; Van Aken & De Boer, 1995). For the ISOW layer below $\sigma_\theta = 27.8$, the highest θ/S concentrations occur along a swath that represents a mixing product primarily between ISOW and LSW, but a fraction of the ISW core also occurs at densities greater than $\sigma_\theta = 27.8$ and therefore occupies a part of what is traditionally defined as the ISOW layer.

In most previous studies of the water mass composition of the ISOW plume, it has been assumed that the waters within the plume are the product of mixing between three primary source waters, or endpoints: (a) NSOW (representing an appropriate volume-weighted mixture of NSDW and NSAIW that overflows the FBC and IFR sills), (b) SPMW that occupies the thermocline layer of the northern Iceland Basin and is initially mixed into the overflows just downstream of the sills, and (c) modified LSW that occupies the intermediate layer in the Iceland Basin and can be subsequently mixed into the plume. Our analysis of the θ/S structure of the plume suggests that a fourth water mass endpoint needs to be taken into account to explain the observed properties of the plume, namely the MEIW, which is the least well constrained component of the dense waters that can overflow the IFR.

In Figure 9b, we show an expanded view of the θ/S distribution in Figure 9a that includes the above mixing endpoints. The core properties of these mixing endpoints are listed in Table S2. Consistent with previous studies (Saunders, 1996; Van Aken & De Boer, 1995), the core properties of ISOW represent a mixture primarily of NSOW and SPMW, with a small degree of influence from LSW. The core of ISW, however, can be seen to lie almost exactly on a straight mixing line between SPMW and MEIW, suggesting to us that the ISW is formed primarily by mixing of MEIW overflowing the sills with SPMW. While previous studies have generally linked the formation of ISW to some mixing process between overflow waters and SPMW, the exact means of its formation has, to our knowledge, not been established, and we believe these observations point to the mixing of MEIW and SPMW as its primary origin. The other possibility, though we feel a less likely one, is that it is formed by preferential mixing of already-formed ISOW with waters in the lower thermocline of the northern Iceland Basin lying along the mixing line between SPWM and LSW with

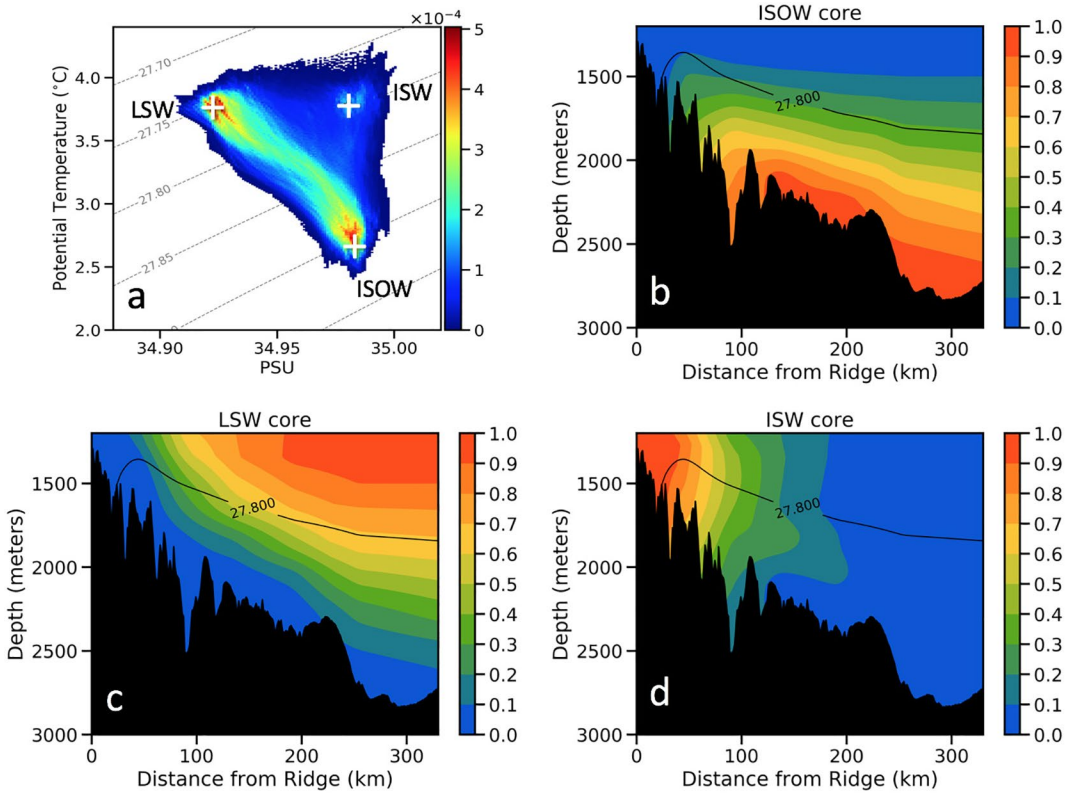

Figure 10. Spatial fractions of the three water mass cores identified in the Iceland-Scotland Overflow Water (ISOW) plume: (a) θ/S frequency distribution within the plume, with crosses denoting local maxima in frequency distribution of the ISOW, Labrador Sea Water (LSW), and Icelandic Slope Water (ISW) cores, (b–d) fractional distributions of the ISOW, LSW, and ISW core waters across the plume, respectively.

potential temperatures near 4.5°C and salinities of 34.98. However, why the ISOW would preferentially mix with these particular waters as it descends the IFR slope to form the core properties of the ISW is hard to understand.

To account for both possibilities, we perform a 3-endpoint water mass decomposition of the waters within the ISOW plume (consisting of mixing only between NSOW, LSW, and SPMW), and a 4-endpoint mixing scheme involving NSOW, MEIW, LSW, and SPMW. For the 3-endpoint mixing scheme, the calculation is straightforward and the set of linear equations that determine the water mass fractions of each source water type is given by:

$$\sum m_i\theta_i = \theta_0 ; \sum m_i S_i = S_0 ; \sum m_i = 1$$

where m_i represent the mass fractions of each water type, θ_i and S_i are the potential temperature and salinity of each water type, and θ_0, S_0 are the observed potential temperature and salinity of the water at any particular location within the plume.

For the 4-endpoint mixing scheme, a unique solution cannot be obtained with only two measured water properties (θ and S), and a further constraint needs to be added to the above equations. To add a fourth constraint to this set of equations, we developed a data-driven approach which uses the same set of equations as above, but is applied instead to the actual ISOW, ISW, and LSW cores in the observed θ/S frequency distributions (i.e., where the θ_i and S_i correspond to the observed potential temperature and salinity of those water mass cores, see Figure 10a), to develop an approximate spatial template for the relative fractions of NSOW and MEIW within the ISOW plume domain. Using these three water mass cores as endpoints in the above system of equations, we can map the respective mass fractions m_i of the water types associated with ISOW, LSW, and ISW water mass cores over the domain of the mooring array, which is shown in Figure 10 for the

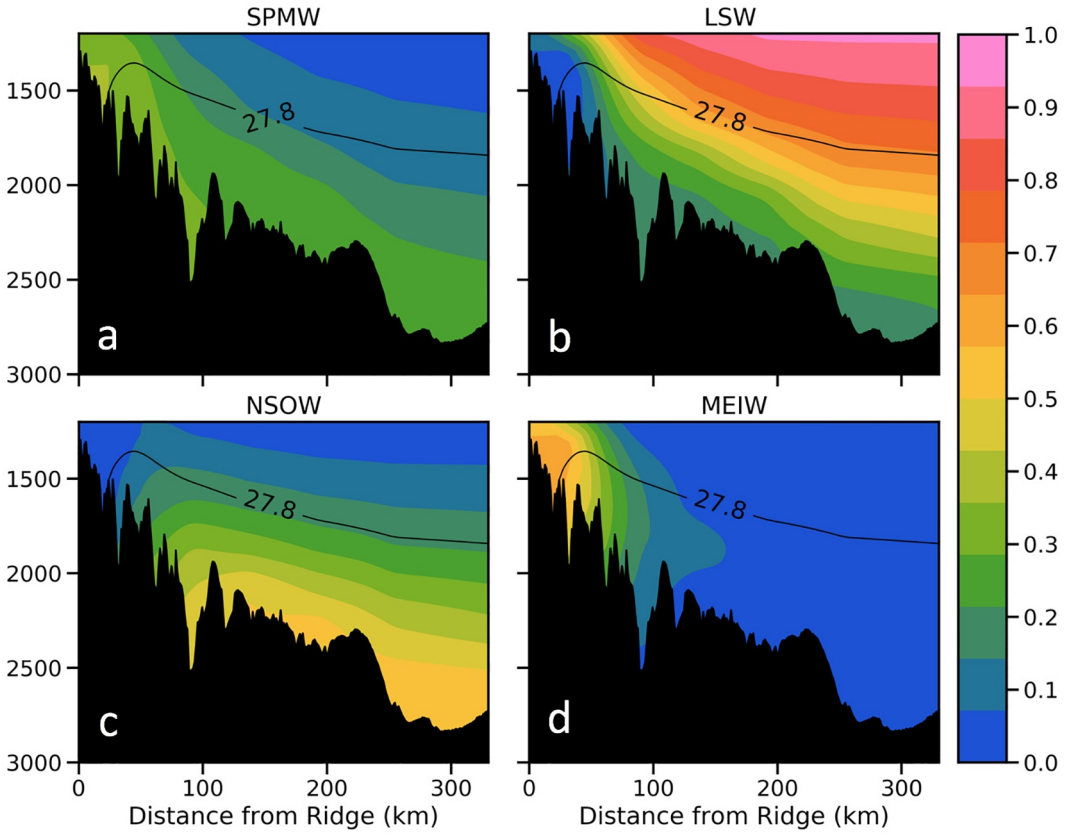

Figure 11. Mean fractions of water mass endpoint mixtures within the Iceland-Scotland Overflow Water plume: (a) Subpolar Mode Water, (b) Labrador Sea Water, (c) Norwegian Sea Overflow Water, (d) Modified East Icelandic Water.

time-mean plume. This analysis shows that the ISOW core waters are found in highest concentration along the bottom in the offshore region of the plume, while the ISW is located along the upper RR slope and also within the base of the ERRC at densities less than $\sigma_\theta = 27.8$, and the LSW is found, as expected, overlying the ISOW layer at intermediate depths. Under the assumption that the ISW reflects mainly a mixing product between MEIW and SPMW, and ISOW mainly a mixing product between NSOW and SPMW, we then use these templates of the ISW and ISOW distributions as a measure (according to their ratio) of the relative fractions of MEIW and NSOW at each location within the plume. This provides a fourth constraint for the 4-endpoint problem, allowing the mass fractions of four original source waters (NSOW, MEIW, SPMW, and LSW) to be calculated across the entire plume domain. While this is not a unique solution, we believe it is the most logical way to approach the 4-endpoint problem given that we only have continuous measurements of two water properties (θ and S) from the array. The corresponding spatial distributions of each of the four source water endpoints are shown in Figure 11 for their time-mean distributions.

The above calculations (for either the 4-endpoint or 3-endpoint problem) are done at each time step (daily), and the respective source water mass fractions at each grid point are then multiplied by the observed velocity at each gridpoint to obtain an estimate of the fractional transport carried by each of the original source waters within the total plume. For the 3-endpoint problem, this calculation yields the result that approximately 46% of the total plume transport, or 2.42 Sv, is associated with "pure" NSOW overflowing the sills (Table 2), and that the remaining transport is made up of 25% SPMW and 29% LSW that are entrained into the plume. For the 4-endpoint calculation, the total transport of overflow waters (NSOW and MEIW) is 2.57 Sv, or 48% of the total plume transport, with 1.81 Sv (34%) being derived from NSOW and 0.76 Sv (14%) from MEIW, and with the remainder being made up of 27% SPMW and 25% LSW. In both cases, approximately half of the total plume transport is derived from the overflow waters and the remaining half from the

Table 2
Water Mass Transports and Respective Water Mass Transport Fractions Within the Iceland-Scotland Overflow Water Plume ($\sigma_\theta > 27.8$)

	3 Endpoint model (SPMW-LSW-NSOW)		4 Endpoint model (SPMW-LSW-NSOW-MEIW)	
Water Mass	Transport (Sv) mean ± std. err.	Fraction (%) mean ± std. err.	Transport (Sv) mean ± std. err.	Fraction (%) mean ± std. err.
SPMW	1.32 ± 0.08	25 ± 2	1.43 ± 0.10 Sv	27 ± 2
LSW	1.56 ± 0.13	29 ± 2	1.31 ± 0.18 Sv	25 ± 3
NSOW	2.42 ± 0.16	46 ± 3	1.81 ± 0.13 Sv	34 ± 2
MEIW	-	-	0.76 ± 0.10 Sv	14 ± 2
Total	5.31 ± 0.35	100	5.31 ± 0.35 Sv	100

Note. Results are shown for the 3-endpoint mixing model (including SPMW, LSW, and NSOW) and the 4-endpoint mixing model (including SPMW, LSW, NSOW, and MEIW).

LSW, Labrador Sea Water; MEIW, Modified East Icelandic Water; NSOW, Norwegian Sea Overflow Water; SPMW, Subpolar Mode Water.

entrained SPWM and LSW, indicating that the overflow source waters approximately double their original transport through the entrainment process.

In addition, the endpoint water mass distributions in Figure 11 indicate a significant fraction of MEIW on the upper RR slope that lies above the $\sigma_\theta = 27.8$ contour, as well as a small influence of NSOW above the $\sigma_\theta = 27.8$ contour in the offshore plume region. This means that some of the original overflow source waters (NSOW and MEIW) have been mixed up into density layers lighter than $\sigma_\theta = 27.8$, or, in other words, that the ISOW layer as it is traditionally defined (i.e., $\sigma_\theta > 27.8$) does not actually capture all of the original overflow source waters. Using the same approach as above to determine the volume-flux weighted contributions by these endpoint water masses, but applied to the velocity distributions and mass fractions of NSOW and MEIW at densities less than $\sigma_\theta = 27.8$, we find that an additional 0.13 Sv of NSOW and 0.53 Sv of MEIW is flowing southward within the upper reaches of the plume (or, in the case of MEIW, within the deep layers of the ERRC along the upper RR slope). For the 3-endpoint solution, involving only NSOW, the corresponding "extra" NSOW transport above $\sigma_\theta = 27.8$ is 0.40 Sv. Note that for the 3-endpoint calculation, the NSOW water mass fraction (not shown) looks very much like a merger of the MEIW and NSOW water mass fractions shown in Figures 11c and 11d, but with slightly weaker relative NSOW fractions on the upper RR slope.

Adding together the volume flux fractions of NSOW and MEIW below $\sigma_\theta = 27.8$ with the above estimates, we obtain a total southward transport of 1.94 Sv of NSOW and 1.29 Sv of MEIW for the 4-endpoint case (for a total overflow transport of 3.23 Sv), and for the 3-endpoint case, a total southward transport of 2.82 Sv of NSOW. The latter estimate is consistent with accepted estimates of the total overflow strength across the Iceland-Scotland Ridge (Table 1), while the former estimate is somewhat larger than accepted estimates and, in particular, requires a much larger contribution of MEIW flowing across the sills than has previously been theorized. We believe the real answer lies somewhere between these two limits, which effectively represent extremes of the possible combinations of NSOW and MEIW that could make up the total overflow. Nevertheless, the total amount of overflow waters inferred from these calculations is consistent with observational estimates of the strength of the net overflow of dense waters through the FBC and across the IFR, within available uncertainties.

In the above water mass decomposition we have neglected a fifth water mass, Lower Deep Water (LDW), that is present in the eastern part of the deep Iceland Basin and has been postulated to mix into the ISOW and enhance its transport through a process known as "cold entrainment" (McCartney, 1992). This water mass enters the deep Iceland Basin from the West European Basin to the south and has slightly lower salinity than ISOW and high dissolved silicate content, indicating its remote origin linked to Antarctic Bottom Waters. The θ/S properties of the deep mooring data in the eastern Iceland Basin clearly show the influence of LDW (Figure 12), where a strong pull of the core ISOW properties toward LDW is seen at the deepest level on mooring M4, and also to a lesser degree at mooring M3. A much smaller influence of LDW is seen

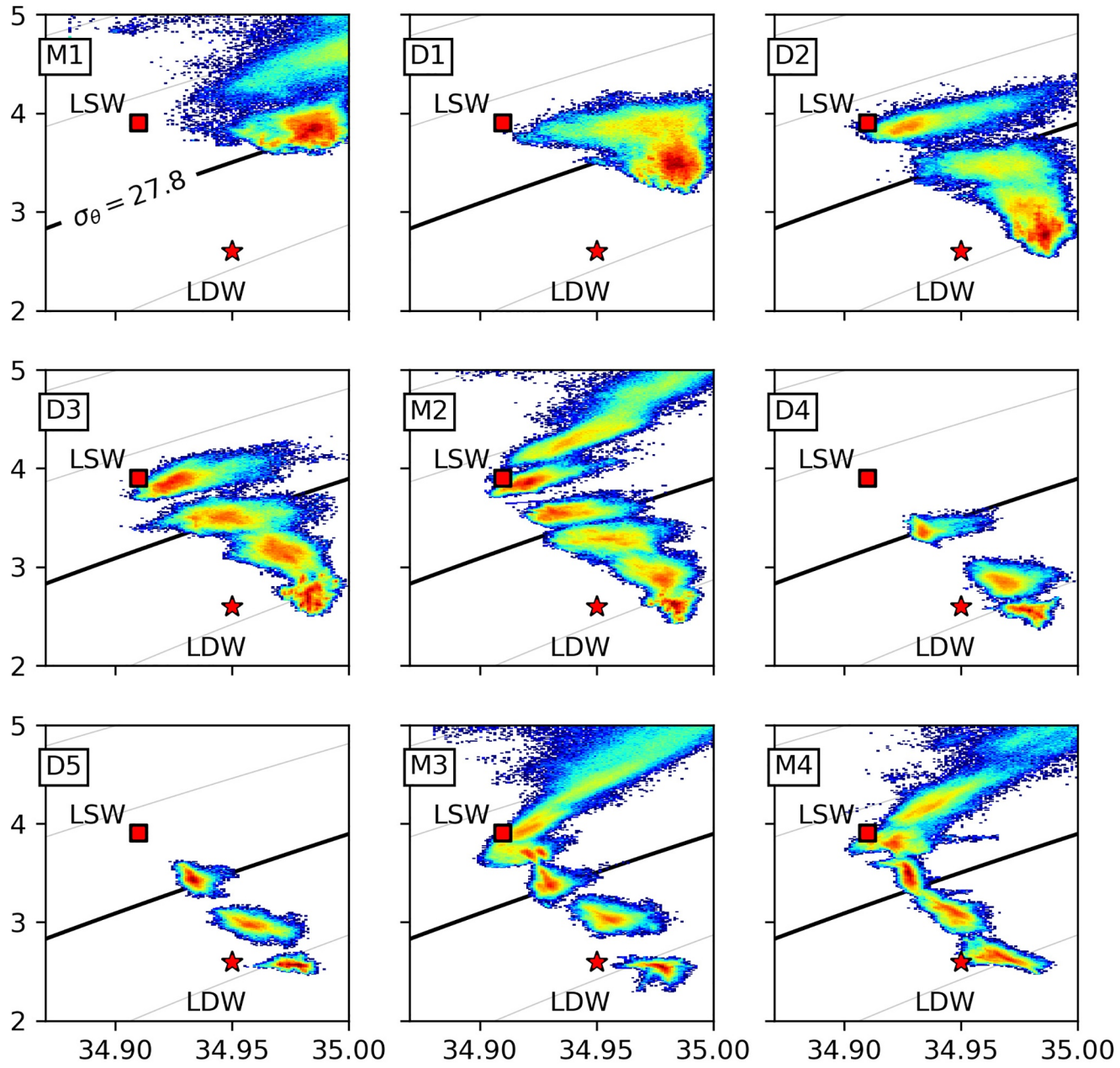

Figure 12. θ/S frequency distributions from individual T/S recorders on each of the moorings across the Iceland Basin, for potential temperatures less than 5°C. Water mass endpoints for Labrador Sea Water (LSW) and Lower Deep Water (LDW) are indicated by the square and starred symbols, respectively.

at moorings D5 and D4, while no LDW influence is seen at moorings M2 or at the shallower moorings along the upper RR slope where most of the ISOW plume transport occurs.

We believe that the northward boundary flow observed at the eastern edge of the Iceland Basin below 2,300 m at mooring M4 (Figure 5 and Table S1) is likely the main entry point for LDW into the Iceland Basin, but that little of this LDW gets mixed into the ISOW that is being exported from the Iceland Basin. As a way to quantify this we can use silicate, which is the most sensitive water mass indicator for LDW, to estimate the fraction of LDW that may be contributing to the deep branch of the plume offshore of mooring M2. Silicate values obtained from a full-chemistry hydrographic section across the OSNAP line at the beginning of the OSNAP program show maximum silicate values of 19 μmol/l in the deep eastern part of the section off Hatton Bank, and values of 11 μmol/l within the ISOW core waters along the mid-RR slope, both of

which are consistent with historically reported values (e.g., Van Aken & De Boer, 1995). The average silicate concentrations in the $\sigma_\theta > 27.8$ layer near the location of moorings D4/D5 are ~12–13 μmol/l, meaning that the fractional LDW contribution to the deep branch of the ISOW plume is at most 25%. Multiplying this by the 0.8 Sv net transport of the deep branch of the ISOW plume gives an estimate of at most 0.2 Sv of LDW contained within the plume, which is a negligible amount compared to the total plume transport of 5.3 Sv.

4. Discussion

These new measurements of the ISOW plume along the OSNAP line raise fundamental questions about our current understanding of the formation and export of ISOW from the Iceland Basin, and its overall role in the lower limb of the Atlantic Meridional Overturning Circulation. First among these is: How can these new, higher transport estimates be rationalized against the lower transports estimated from previous moored array studies of the ISOW plume in the northern Iceland Basin?

One possibility is time-dependence of the overflow itself, and whether it may have been larger during the time of these observations than during the corresponding periods of the earlier studies. We believe this is unlikely, since the long-term measurements of the FBC overflow by Hansen et al. (2016) show yearly average variations about the long-term mean overflow of no more than 0.3 Sv. Those overflow observations include the time period of the Knzow and Zenk (2014) study (collected during 2000–2002) but not the time period (1990–1991) of the measurements described by Saunders (1996). Therefore, it is possible that the overflow could have been anomalously weak during the period of the Saunders (1996) study, and it must also be acknowledged that little is known of the interannual variability of the remaining overflow across the IFR. However, the magnitude of the overflow reduction during these periods would have to have been of order 1 Sv to explain the discrepancy between our results and those of Saunders (1996) and Kanzow and Zenk (2014), which does not seem likely in view of the existing overflow observations.

A second possibility is that significant additional entrainment occurs within the ISOW plume as it flows southward from the northern Iceland basin toward the OSNAP line. A related study of the DWBC off East Greenland (Lauderdale et al., 2008) found elevated mixing rates in the DSOW core layer near Cape Farewell and suggested that up to 5 Sv of additional entrainment could occur in the East Greenland DWBC due to vertical mixing that takes place downstream of the rapid DSOW entrainment region a few hundred km from Denmark Strait. The authors did not explicitly account for the addition of ISOW to the DWBC off East Greenland, of perhaps 3 Sv, or any possible recirculation of deep waters of the Irminger Basin into the DWBC, so that a more probable estimate of this additional entrainment would be of the order 1–2 Sv. Whether such additional entrainment could be occurring in the ISOW plume is unclear, but if it was indeed occurring, it would imply additional dilution of the ISOW layer (mainly with LSW), and one would expect to see corresponding changes in the ISOW core properties (θ, S, and σ_θ) along its southward pathway from Iceland. There is really no evidence for this taking place, however. Saunders (1996) and multiple other studies (e.g., Fogelqvist et al., 2003; Hansen & Østerhus, 2000), as well as hydrographic data from the "Ellet line" line south of Iceland acquired during the period of our study (https://www.bodc.ac.uk/data/bodc_database/nodb/cruise/15037/) show that after its initial rapid entrainment phase the ISOW core has θ/S properties all along the RR slope south of Iceland that are very similar to our observed ISOW core properties of ~[2.6–2.7°C, 34.9]. Therefore, substantial modification of the ISOW core waters following the rapid entrainment phase downstream of the FBC does not appear to occur.

There are, however, notable differences in the characteristics of the ISOW plume along its southward pathway between the Saunders (1996), Kanzow and Zenk (2014) and OSNAP arrays. The maximum mean speeds in the plume gradually decrease (from nearly 0.2 m/s at the Saunders array, to ~0.15 m/s at the Kanzow & Zenk array, and ~0.1 m/s at the OSNAP array), and the average thickness of the $\sigma_\theta > 27.8$ layer also increases substantially between the arrays. Comparing Figure 6a with similar representations of the plume structure shown in Saunders (1996) and Kanzow and Zenk (2014), we estimate the average thickness of the near-bottom $\sigma_\theta > 27.8$ layer to be 280, 340, and 450 m at the three arrays, respectively, where these estimates are taken from the point where the $\sigma_\theta = 27.8$ contour intersects the RR or Iceland slope topography to a depth of 2,400 m (spanning the main area of active plume flow in each case and to the maximum bottom depth of the Saunders array section). This suggests that there could be a

mixing-related "inflation" of the ISOW layer and, possibly, a corresponding transport increase due to upward mixing of momentum from the bottom layer, which slows in its maximum speeds as the plume moves southward.

Enhanced mixing within the ISOW plume could be produced as it encounters increasingly rugged topography along the eastern flank of the RR upstream of the OSNAP line (see Figure 1). The structure of the density field within the ISOW plume at the OSNAP line—in particular the downward bowing of density surfaces int the crest of the RR, as noted earlier—is indeed suggestive of enhanced bottom-intensified mixing over the upper ridge flank. This feature is consistently present in all of our OSNAP hydrographic sections (e.g., Figure 2), and also in the OVIDE hydrographic data across the region of our array (Daniault et al., 2016), but does not appear to be present at the Saunders or Kanzow & Zenk array locations. Therefore, it appears to develop as the plume begins to encounter the rougher RR topography going southward. However, any additional entrainment that results from this enhanced mixing does not seem to impact the core properties of ISOW near the bottom, but instead may act to entrain additional LSW into the upper parts of the plume.

Finally, we consider whether the earlier arrays by Saunders and Kanzow & Zenk could have underestimated the transport of the ISOW plume, or if our array may have overestimated its transport. For both ours and Saunders' arrays, the average separation between moorings over the region where most of the plume flow is contained is approximately 40 km, while for the Kanzow & Zenk array it was almost twice that (70–80 km). Furthermore, the "I" mooring in Kanzow & Zenk's "ISOW" array (see Figure 1) was not recovered, so that the authors had to infer the flow in the upper part of the ISOW plume from a single RAFOS float trajectory that passed through the region during the time of their study. These earlier studies also had far fewer current meters located within the southward flowing ISOW layer than in the OSNAP array: seven in the Saunders array, and five in the Kanzow & Zenk array, compared to 14 in the OSNAP array (Figure 6a). Given the sparse spatial sampling of the Kanzow & Zenk array, it seems possible that the flow maximum of the ISOW plume could have been missed and the transport underestimated. In the case of Saunders' study, the near-bottom current meters in that array were placed at 10 m above bottom, and five of the seven current meters that recorded southward flow in the ISOW layer were from those current meters at 10 m above bottom. These near-bottom current meters—using the method applied by Saunders, in which representative cross-sectional areas were assigned to each current meter—accounted for 2.3 Sv (72%) of the total of 3.2 Sv ISOW transport estimated by Saunders. If these near-bottom current meters were within the bottom boundary layer, which seems likely, it could have led to an underestimate of the plume's transport. Therefore, we believe that there are legitimate reasons why the earlier arrays by Saunders and Kanzow & Zenk could have both underestimated the ISOW plume's transport. In addition, as noted previously, Saunders' water mass analysis of the ISOW plume could account for only 1.6 Sv of dense overflow waters within the plume, less than even the ~2.0 Sv known to be flowing through the FBC.

As to whether the OSNAP array could have overestimated the ISOW plume's transport, such a scenario could occur if the moorings happened to be placed in local maxima of the flow with regions of weaker flow between them. The only mooring location where we think such a situation could apply is at D2, which lies in an off-axial trough associated with the so-called V-shaped ridge/trough system emanating from the RR's main spreading center (Jones et al., 2002; see Figure 1). Mooring D2 was specifically placed in this deep trough to capture any ISOW flow that might be funneled along it. Although there is clearly ISOW flow within and overlying this deep trough, the maximum of the plume flow is found at different locations along the slope at different times (Figures 5 and S1) and the flow at mooring D2 can even stop or reverse. Therefore, we do not believe that the OSNAP mooring placements along the RR topography are likely to have led to any significant transport bias due to having been preferentially located in regions of stronger flow. Also, as shown previously, the available transport estimates from contemporaneous CTD/LADCP sections across the plume show relatively good agreement with the moored transport estimates.

We therefore conclude that the apparent transport growth of the ISOW plume could be due, in part, to possible underestimates of the plume strength in earlier studies, and also possibly to the effects of gradual additional entrainment of LSW into the top of the plume between the southern Icelandic slope and the southern tip of the RR.

Given the larger transport estimate for the ISOW plume obtained in this study compared to earlier studies, another important question is: What do these higher transport estimates imply about the known export pathways of ISOW from the Iceland Basin? Historically, it has been assumed that most of the ISOW plume exits the Iceland Basin through fracture zones in the Mid-Atlantic Ridge, flowing into the Irminger Basin and then wrapping around the northern rim of that basin to join the DWBC system off east Greenland (Dickson et al., 2008). The most important of these fracture zones is the Charlie-Gibbs Fracture Zone (CGFZ) near 53°N (Figure 13), where observations by Saunders (1994), and later by Bower and Furey (2017), have estimated that between 1.7 and 2.4 Sv of ISOW flows westward into the Irminger Basin. A second fracture zone farther north along the ridge, the Bight Fracture Zone (BFZ) near 57°N, has also been viewed as a potentially significant cross-ridge pathway for ISOW, and recent moored observations in the BFZ by Furey et al. (2020) found a 2-year mean transport of ISOW of 0.8 ± 0.4 Sv through the BFZ. These estimates are generally consistent with results from recent modeling studies that show about 3 Sv of ISOW flowing through various gaps in the Mid-Atlantic Ridge, including the CGFZ, BFZ, and a few smaller gaps between 55 and 56°N (Xu et al., 2010, 2018). Notably, these estimates are also consistent with the earlier estimates of just over 3 Sv for the ISOW plume in the Iceland Basin, having reinforced the impression that most of the ISOW plume flow exited the Iceland Basin through gaps in the ridge to flow into the western basin of the Atlantic Ocean.

However, our new measurements of the ISOW plume showing a transport of over 5 Sv means that there must be another—relatively significant—pathway for ISOW to leave the Iceland Basin. The only other pathway for ISOW to exit the Iceland Basin is southward along the east side of the Mid-Atlantic Ridge into the West European Basin, bypassing the CGFZ. Indeed, there have been previous indications that some of the ISOW flow has to follow this pathway, based on water mass analysis showing a clear imprint of ISOW properties in the West European Basin that can be traced as far south as the Madeira Abyssal Plain (Van Aken, 2000). Zou et al. (2017) also found evidence of a significant southward flow into the West European Basin along the eastern flank of the Mid-Atlantic Ridge from yearlong current meter records deployed in the ISOW layer. In addition to the main ISOW plume flowing along the RR, there is a small contribution of ISOW that can enter the West European Basin through the Rockall Trough after overflowing the Wyville-Thompson Ridge, but this contribution to the net export of ISOW from the Iceland Basin is thought to be small, of order 0.1–0.3 Sv (Sherwin & Turrell, 2005). Based on chlorofluoromethane (CFC-11) inventories, LeBel et al. (2008) estimated a mean production rate of ISOW of 5.7 Sv for the period between 1970-1997, and found that 30% of the ISOW CFC-11 inventory was in the eastern basin of the Atlantic, suggesting that about one-third (equivalent to ∼1.7 Sv) of the ISOW export from the Iceland Basin must follow this eastern pathway. Using CFC-11 and tritium observations, Fleischmann et al. (2001) found that as much as 2.4–3.5 Sv of ISOW could be flowing into the West European Basin along this pathway. These estimates, along with our updated estimate of the ISOW plume transport at the OSNAP line, and other observational estimates of the ISOW plume transport and its export pathways from the Iceland Basin, are summarized in Figure 13. The recent modeling study of Xu et al. (2018) also reproduces a significant southward pathway of ISOW along the eastern flank of the Mid-Atlantic Ridge, of 1.7 Sv, that is composed of the densest ISOW waters flowing from the Iceland Basin.

We find it compelling that our new estimate of the net export of ISOW from the Iceland Basin, of 5.3 ± 0.4 Sv, is in relatively close agreement with estimated net production of ISOW by LeBel et al. (2008). Both studies indicate (Lebel et al.'s by CFC-11 inventories, and ours by inference relative to other known exit pathways) that approximately 2 Sv of the ISOW plume transport follows this eastern pathway into the West European Basin. The remainder, of order 3 Sv, flows to the western basin through gaps in the Mid-Atlantic Ridge, consistent with the available observations from CGFZ and BFZ. We believe that these results, together with our water mass analysis of the ISOW plume, which shows that it contains approximately 3 Sv of pure overflow waters and nearly doubles its transport through entrainment, paint a fairly self-consistent picture of the mass budget of ISOW in the eastern North Atlantic. The principal outcome of this new understanding is that the ISOW, through both its eastern and western pathways, plays a larger role in the lower limb of the AMOC than has commonly been perceived.

It remains an interesting question what happens to this eastern pathway of ISOW. Does it continue southward in the eastern basin, or does it find a pathway back to the western basin at some more southerly

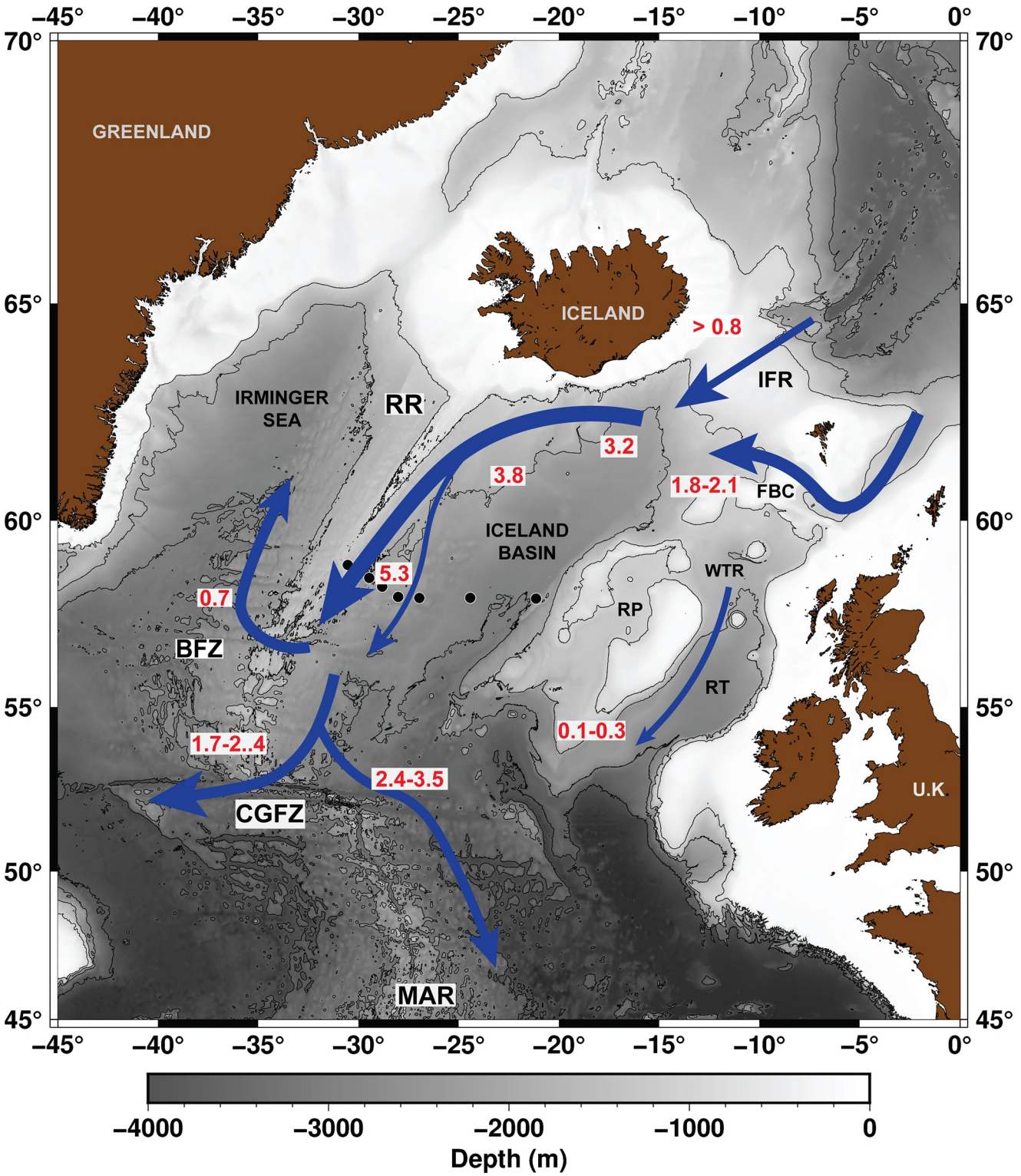

Figure 13. Iceland-Scotland Overflow Water pathways and transports in the eastern subpolar North Atlantic (adapted from Zou et al., 2017). All transports labeled in boxes (in Sv) are from observation-based estimates; data sources and references for each location are described in the text. Dots indicate the location of the Overturning in the Subpolar North Atlantic Program Iceland Basin mooring array. Abbreviations: FBC = Faroe Bank Channel; IFR = Iceland-Faroes Ridge; RR = Reykjanes Ridge; WTR = Wyville-Thompson Ridge; RT = Rockall Trough; RP = Rockall Plateau; BFZ = Bight Fracture Zone; CGFZ = Charlie Gibbs Fracture Zone; MAR = Mid-Atlantic Ridge.

latitude? The CFC-11 inventories by LeBel et al. (2008)—though limited by the time horizon of CFC input to the ocean—suggest a possible route back to the western basin south of the Azores along a zonal pathway near 30°N. This pathway would be very similar to the recently identified pathway of Labrador Sea Water that passes into the eastern basin through the CGFZ, southward in the eastern basin, and then re-crosses the Mid-Atlantic Ridge south of the Azores to flow westward along ~30°N, eventually joining the DWBC off of the Bahamas (Bilo & Johns, 2019). Given the mounting evidence for this eastern pathway of ISOW, more research into its eventual fate seems warranted.

5. Conclusions

We report here the results from a moored array along the eastern flank of the Reykjanes Ridge measuring the ISOW plume and its southward export of overflow and entrained waters from the Iceland Basin over a 4-year period from 2014 to 2018. This array is part of the Overturning in the Subpolar North Atlantic Program (OSNAP) trans-basin observing system and represents the most comprehensive array yet deployed across the ISOW plume. The main conclusions of this study are as follows:

1. At the location of the OSNAP array, near 58°N, the ISOW plume consists of two branches, a main branch flowing along the upper Reykjanes Ridge slope in depths from 1,400 to 2,200 m and a lower branch at depths of 2,400–2,800 m along the deeper ridge flank. The total transport of the two branches is 6.1 ± 0.3 Sv (for $\sigma_\theta > 27.8$), and the net export of ISOW from the Iceland Basin is 5.3 ± 0.4 Sv after accounting for interior recirculation across the basin.
2. Water mass analysis of the ISOW plume shows that about half of its transport is made up of overflow waters crossing the Iceland-Scotland Ridge and the other half from entrained waters, with the entrained waters being a nearly 50/50 mix of SPMW and LSW. The Iceland- Scotland overflow therefore nearly doubles its transport through entrainment.
3. Our observations also show that some fraction of the original overflow waters (NSOW and MEIW) are mixed up into layers lighter than $\sigma_\theta = 27.8$, meaning that the ISOW layer as traditionally defined ($\sigma_\theta > 27.8$) does not actually contain all of the overflow waters. The total amount of overflow waters (NSOW and MEIW) transported southward in the ISOW plume and the lower part of the ERRC is found to be approximately 3 Sv, consistent with existing estimates of the total overflow across the ISR. Our analysis further suggests that MEIW may be a more important component of the overflow than previously thought, contributing not only to the ISOW plume at densities $\sigma_\theta > 27.8$ but also being a key water mass component in the formation of Icelandic Slope Water that is present all along the upper Reykjanes Ridge slope south of Iceland.
4. The transport of the ISOW plume derived from this array is larger than previously accepted estimates of 3–4 Sv from earlier studies, including those from moored arrays farther north in the Iceland Basin. Part of this transport growth may be real and related to enhanced mixing in the ISOW plume as it encounters more rugged topography along its southward pathway, while part of it could be due to underestimates of the ISOW plume transport from earlier studies. The estimate of 5.3 Sv we obtain for the net export of ISOW from the Iceland Basin is more consistent with independent estimates of ISOW production from tracer inventories than the earlier estimates.
5. The larger ISOW transport obtained from these observations implies that a significant additional pathway for ISOW must exist, of order 2 Sv, that bypasses the Charlie Gibbs Fracture Zone and other gaps in the Mid-Atlantic Ridge to flow southward into the eastern basin of the Atlantic. The existence of this pathway is also inferred from hydrographic and tracer observations and has been found in recent numerical model simulations.

The observations reported here are from the first 4 years (2014–2018) of the OSNAP Iceland Basin array, and further updates to these results will be forthcoming as OSNAP is extended; it is currently planned to continue until at least 2024. Besides the observations of the ISOW plume described here, the basin-wide OSNAP array provides continuous measurements across the other major deep boundary current systems of the subpolar gyre—including the DWBC off east Greenland (Hopkins et al., 2019), west Greenland (Pacini et al., 2020), and in the Labrador Sea (Zantopp et al., 2017)—so that an integrated, long-term analysis of the transports of the deep limb of the AMOC around the entire subpolar North Atlantic can be achieved. The subpolar North Atlantic is currently undergoing remarkable changes, having recently experienced the largest freshening

event in the upper eastern subpolar basin observed in the past 120 years (Holliday et al., 2020). It is anticipated that this freshening event will propagate into the ISOW system through entrainment, or eventually through changes in the source water properties of the overflows across the Iceland-Scotland Ridge, and that the observations collected during the OSNAP time frame will aid in understand how such water mass anomalies are introduced into and propagate within the DWBC system of the subpolar gyre.

Data Availability Statement

OSNAP data used in this study are available online at http://www.o-snap.org/observations/data/. The Ssalto/Duacs altimeter products used in this study were produced and distributed by the Copernicus Marine and Environment Monitoring Service (CMEMS): http://www.marine.copernicus.eu. The gridded Argo analysis used in this study can be accessed from the University of Miami's Scholarly Repository at https://doi.org/10.17604/cf5z-x124.

Acknowledgments
The authors would like to thank the captains and crews of the R/V Knorr, R/V Pelagia, RRS Discovery, and R/V Neil Armstrong, as well as the University of Miami Ocean Technology Group, for their able assistance in the seagoing operations supporting this research. Financial support for this research was provided by the U.S. National Science Foundation under grants OCE-1259398 and OCE-1756231. S. Zou acknowledges support by the U.S. National Science Foundation under grant OCE-1756361. Acknowledgment is also extended to C. Böning and A. Biastoch for providing FLAME model output. We would also like to acknowledge two anonynous reviewers for their helpful comments on the manuscript.

References

Akima, H. (1970). A new method of interpolation and smooth curve fitting based on local procedures. *Journal of the ACM*, *17*(4), 589–602. https://doi.org/10.1145/321607.321609

Baringer, M. O. N., & Price, J. F. (1997). Mixing and spreading of the mediterranean outflow. *Journal of Physical Oceanography*, *27*(8). https://doi.org/10.1175/1520-0485(1997)027<1654:MASOTM>2.0.CO;2

Beaird, N. L., Rhines, P. B., & Eriksen, C. C. (2013). Overflow waters at the Iceland-Faroe Ridge observed in multiyear Seaglider Surveys. *Journal of Physical Oceanography*, *43*(11), 2334–2351. https://doi.org/10.1175/jpo-d-13-029.1

Bilo, T. C., & Johns, W. E. (2019). Interior pathways of Labrador Sea water in the North Atlantic from the Argo perspective. *Geophysical Research Letters*, *46*(6), 3340–3348. https://doi.org/10.1029/2018gl081439

Bower, A. S., & Furey, H. (2017). Iceland-Scotland Overflow Water transport variability through the Charlie-Gibbs Fracture Zone and the impact of the North Atlantic Current. *Journal of Geophysical Research: Oceans*, *122*(9), 6989–7012. https://doi.org/10.1002/2017JC012698

Bower, A. S., Lozier, M. S., Gary, S. F., & Boning, C. W. (2009). Interior pathways of the North Atlantic meridional overturning circulation. *Nature*, *459*(7244), 243–247. https://doi.org/10.1038/nature07979

Callies, J., & Ferrari, R. (2018). Dynamics of an abyssal circulation driven by bottom-intensified mixing on slopes. *Journal of Physical Oceanography*, *48*(6), 1257–1282. https://doi.org/10.1175/JPO-D-17-0125.1

Daniault, N., Mercier, H., Lherminier, P., Sarafanov, A., Falina, A., Zunino, P., et al. (2016). The northern North Atlantic Ocean mean circulation in the early 21st century. *Progress in Oceanography*, *146*, 142–158. https://doi.org/10.1016/j.pocean.2016.06.007

De Jong, M. F., Oltmanns, M., Karstensen, J., & De Steur, L. (2018). Deep convection in the Irminger Sea observed with a dense mooring array. *Oceanography*, *31*(1), 50–59. https://doi.org/10.5670/oceanog.2018.109

Dickson, R. R., Meincke, J., & Rhines, P. (2008). *Arctic-Subarctic ocean fluxes: Defining the role of the northern seas in climate*. https://doi.org/10.1007/978-1-4020-6774-7

Dietrich, G. (1956). Overflow over the Iceland-Färoes ridge near the sea bottom as observed during the cruises of the research ship "Anton Dohrn" 1955/56, *Deutsche Hydrographische Zeitschrift*, *9*(2), 78–90. https://doi.org/10.1007/bf02021146

Fleischmann, U., Hildebrandt, H., Putzka, A., & Bayer, R. (2001). Transport of newly ventilated deep water from the Iceland Basin to the Westeuropean Basin. *Deep-Sea Research Part I: Oceanographic Research Papers*, *48*(8), 1793–1819. https://doi.org/10.1016/S0967-0637(00)00107-2

Fogelqvist, E., Blindheim, J., Tanhua, T., Østerhus, S., Buch, E., & Rey, F. (2003). Greenland-Scotland overflow studied by hydro-chemical multivariate analysis. *Deep-Sea Research Part I: Oceanographic Research Papers*, *50*(1), 73–102. https://doi.org/10.1016/S0967-0637(02)00131-0

Furey, H. H., Bower, A. S., Johns, W. E., Houk, A., & Ramsey, A. (2020). The variability of the deep bight: Two-years of moored observations in the bight fracture zone. In *Ocean Sciences Meeting 2020*. AGU.

Ganachaud, A. (2003). Error budget of inverse box models: The North Atlantic. *Journal of Atmospheric and Oceanic Technology*, *20*(11), 1641–1655. https://doi.org/10.1175/1520-0426(2003)020<1641:eboibm>2.0.co;2

García-Ibáñez, M. I., Pérez, F. F., Lherminier, P., Zunino, P., Mercier, H., & Tréguer, P. (2018). Water mass distributions and transports for the 2014 GEOVIDE cruise in the North Atlantic. *Biogeosciences*, *15*(7), 2075–2090. https://doi.org/10.5194/bg-15-2075-2018

Gupta, M. M. (1991). Numerical methods and software (David Kahaner, Cleve Moler, and Stephen Nash). *SIAM Review*, *33*(1), 144–147. https://doi.org/10.1137/1033033

Hansen, B., Larsen, K. M. H., Hatun, H., & Osterhus, S. (2016). A stable Faroe Bank Channel overflow 1995-2015. *Ocean Science*, *12*(6), 1205–1220. https://doi.org/10.5194/os-12-1205-2016

Hansen, B., Margretha Húsgar Larsen, K., Malskær Olsen, S., Quadfasel, D., Jochumsen, K., & Østerhus, S. (2018). Overflow of cold water across the Iceland-Faroe Ridge through the Western Valley. *Ocean Science*, *14*(4), 871–885. https://doi.org/10.5194/os-14-871-2018

Hansen, B., & Østerhus, S. (2000). North Atlantic-Nordic Seas exchanges. *Progress in Oceanography*, *45*, 109–208. https://doi.org/10.1016/S0079-6611(99)00052-X

Hansen, B., & Osterhus, S. (2007). Faroe Bank Channel overflow 1995-2005. *Progress in Oceanography*, *75*(4), 817–856. https://doi.org/10.1016/j.pocean.2007.09.004

Holliday, N. P., Bersch, M., Berx, B., Chafik, L., Cunningham, S., Florindo-López, C., et al. (2020). Ocean circulation causes the largest freshening event for 120 years in eastern subpolar North Atlantic. *Nature Communications*, *11*(1). https://doi.org/10.1038/s41467-020-14474-y

Hopkins, J. E., Holliday, N. P., Rayner, D., Houpert, L., Le Bras, I., Straneo, F., et al. (2019). Transport variability of the Irminger Sea deep western boundary current from a Mooring Array. *Journal of Geophysical Research: Oceans*, *124*, 3246–3278. https://doi.org/10.1029/2018JC014730

Jochumsen, K., Köllner, M., Quadfasel, D., Dye, S., Rudels, B., & Valdimarsson, H. (2015). On the origin and propagation of Denmark Strait Overflow Water anomalies in the Irminger Basin. *Journal of Geophysical Research: Oceans*, *120*(3), 1841–1855. https://doi.org/10.1002/2014JC010397

Jochumsen, K., Moritz, M., Nunes, N., Quadfasel, D., Larsen, K. M. H., Hansen, B., et al. (2017). Revised transport estimates of the Denmark Strait overflow. *Journal of Geophysical Research: Oceans*, *122*(4), 3434–3450. https://doi.org/10.1002/2017jc012803

Jones, S. M., White, N., & Maclennan, J. (2002). V-shaped ridges around Iceland: Implications for spatial and temporal patterns of mantle convection. *Geochemistry, Geophysics, Geosystems*, *3*(10), 1–23. https://doi.org/10.1029/2002GC000361

Kanzow, T., & Zenk, W. (2014). Structure and transport of the Iceland Scotland Overflow plume along the Reykjanes Ridge in the Iceland Basin. *Deep Sea Research Part I: Oceanographic Research Papers*, *86*, 82–93. https://doi.org/10.1016/j.dsr.2013.11.003

Kieke, D., Rhein, M., Stramma, L., Smethie, W. M., Bullister, J. L., & LeBel, D. A. (2007). Changes in the pool of Labrador Sea Water in the subpolar North Atlantic. *Geophysical Research Letters*, *34*(6). https://doi.org/10.1029/2006GL028959

Kieke, D., & Yashayaev, I. (2015). Studies of Labrador Sea Water formation and variability in the subpolar North Atlantic in the light of international partnership and collaboration. *Progress in Oceanography*, *132*, 220–232. https://doi.org/10.1016/j.pocean.2014.12.010

Koman, G., Johns, W. E., & Houk, A. (2020). Transport and evolution of the East Reykjanes Ridge Current. *Journal of Geophysical Research: Oceans*, *125*(10). https://doi.org/10.1029/2020JC016377

Lauderdale, J. M., Bacon, S., Garabato, A. C. N., & Holliday, N. P. (2008). Intensified turbulent mixing in the boundary current system of southern Greenland. *Geophysical Research Letters*, *35*(4). https://doi.org/10.1029/2007GL032785

LeBel, D. A., Smethie, W. M., Rhein, M., Kieke, D., Fine, R. A., Bullister, J. L., et al. (2008). The formation rate of North Atlantic Deep Water and Eighteen Degree Water calculated from CFC-11 inventories observed during WOCE. *Deep-Sea Research Part I: Oceanographic Research Papers*, *55*(8), 891–910. https://doi.org/10.1016/j.dsr.2008.03.009

Lozier, M. S., Li, F., Bacon, S., Bahr, F., Bower, A. S., Cunningham, S. A., et al. (2019). A sea change in our view of overturning in the subpolar North Atlantic. *Science*, *363*(6426), 516–521. https://doi.org/10.1126/science.aau6592

McCarthy, G. D., Brown, P. J., Flagg, C. N., Goni, G., Houpert, L., Hughes, C. W., et al. (2020). Sustainable observations of the AMOC: Methodology and technology. *Reviews of Geophysics*, *58*. https://doi.org/10.1029/2019RG000654

McCarthy, G. D., Smeed, D. A., Johns, W. E., Frajka-Williams, E., Moat, B. I., Rayner, D., et al. (2015). Measuring the Atlantic meridional overturning circulation at 26 degrees N. *Progress in Oceanography*, *130*, 91–111. https://doi.org/10.1016/j.pocean.2014.10.006

McCartney, M. S. (1992). Recirculating components to the deep boundary current of the Northern North-Atlantic. *Progress in Oceanography*, *29*(4), 283–383. https://doi.org/10.1016/0079-6611(92)90006-l

Olsen, S. M., Hansen, B., Østerhus, S., Quadfasel, D., & Valdimarsson, H. (2016). Biased thermohaline exchanges with the Arctic across the Iceland-Faroe Ridge in ocean climate models. *Ocean Science*, *12*(2), 545–560. https://doi.org/10.5194/os-12-545-2016

Osterhus, S., Sherwin, T., Quadfasel, D., & Hansen, B. (2008). The overflow transport east of Iceland. In *Arctic-subarctic ocean fluxes: Defining the role of the northern seas in climate*. https://doi.org/10.1007/978-1-4020-6774-7_19

Pacini, A., Pickart, R. S., Bahr, F., Torres, D. J., Ramsey, A. L., Holte, J., et al. (2020). Mean conditions and seasonality of the west Greenland boundary current system near Cape Farewell. *Journal of Physical Oceanography*, *50*(10), 2849–2871. https://doi.org/10.1175/JPO-D-20-0086.1

Peters, H., Johns, W. E., Bower, A. S., & Fratantoni, D. M. (2005). Mixing and entrainment in the Red Sea outflow plume. Part I: Plume structure. *Journal of Physical Oceanography*, *35*(5), 569–583. https://doi.org/10.1175/JPO2679.1

Read, J. F. (2000). CONVEX-91: Water masses and circulation of the Northeast Atlantic subpolar gyre. *Progress in Oceanography*, *48*, 461–510. https://doi.org/10.1016/S0079-6611(01)00011-8

Rhein, M., Kieke, D., Hüttl-Kabus, S., Roessler, A., Mertens, C., Meissner, R., et al. (2011). Deep water formation, the subpolar gyre, and the meridional overturning circulation in the subpolar North Atlantic. *Deep-Sea Research Part II: Topical Studies in Oceanography*, *58*(17–18), 1819–1832. https://doi.org/10.1016/j.dsr2.2010.10.061

Saunders, P. M. (1994). The flux of overflow water through the Charlie-Gibbs fracture-zone. *Journal of Geophysical Research*, *99*(C6), 12343–12355. https://doi.org/10.1029/94jc00527

Saunders, P. M. (1996). The flux of dense cold overflow water southeast of Iceland. *Journal of Physical Oceanography*, *26*(1), 85–95. https://doi.org/10.1175/1520-0485(1996)026<0085:tfodco>2.0.co;2

Sherwin, T. J., & Turrell, W. R. (2005). Mixing and advection of a cold water cascade over the Wyville Thomson Ridge. *Deep-Sea Research Part I: Oceanographic Research Papers*, *52*(8), 1392–1413. https://doi.org/10.1016/j.dsr.2005.03.002

Sibson, R. (1981). A brief description of natural neighbour interpolation. In *Interpreting multivariate data*.

Smith, W. H. F., & Sandwell, D. T. (1997). Global seafloor topography from satellite altimetry and ship depth soundings. *Science*, *277*, 1957–1962. https://doi.org/10.1126/science.277.5334.1956

Steele, J. H., Barrett, J. R., & Worthington, L. V. (1962). Deep currents south of iceland. *Deep-Sea Research and Oceanographic Abstracts*, *9*(11–12), 465–474. https://doi.org/10.1016/0011-7471(62)90097-9

St Laurent, L. C., Toole, J. M., & Schmitt, R. W. (2001). Buoyancy forcing by turbulence above rough topography in the abyssal Brazil Basin. *Journal of Physical Oceanography*, *31*(12). https://doi.org/10.1175/1520-0485(2001)031<3476:BFBTAR>2.0.CO;2

Tozer, B., Sandwell, D. T., Smith, W. H. F., Olson, C., Beale, J. R., & Wessel, P. (2019). Global bathymetry and topography at 15 arc sec: SRTM15+. *Earth and Space Science*, *6*. https://doi.org/10.1029/2019EA000658

Van Aken, H. M. (2000). The hydrography of the mid-latitude northeast Atlantic Ocean I: The deep water masses. *Deep-Sea Research Part I: Oceanographic Research Papers*, *47*(5), 757–788. https://doi.org/10.1016/S0967-0637(99)00092-8

Van Aken, H. M., & De Boer, C. J. (1995). On the synoptic hydrography of intermediate and deep water masses in the Iceland Basin. *Deep-Sea Research Part I*, *42*(2), 42–189. https://doi.org/10.1016/0967-0637(94)00042-Q

Watson, D. F. (1992). Contouring: A guide to the analysis and display of spatial data. In *Contouring: A guide to the analysis and display of spatial data*. https://doi.org/10.1016/0098-3004(93)90069-h

Xu, X., Bower, A., Furey, H., & Chassignet, E. P. (2018). Variability of the Iceland-Scotland overflow water transport through the Charlie-Gibbs fracture zone: Results from an Eddying simulation and observations. *Journal of Geophysical Research: Oceans*, *123*(8), 5808–5823. https://doi.org/10.1029/2018JC013895

Xu, X., Schmitz, W. J., Hurlburt, H. E., Hogan, P. J., & Chassignet, E. P. (2010). Transport of Nordic Seas overflow water into and within the Irminger Sea: An eddy-resolving simulation and observations. *Journal of Geophysical Research*, *115*(12). https://doi.org/10.1029/2010JC006351

Yashayaev, I., & Loder, J. W. (2016). Recurrent replenishment of Labrador Sea Water and associated decadal-scale variability. *Journal of Geophysical Research: Oceans*, *121*(11), 8095–8114. https://doi.org/10.1002/2016JC012046

Zantopp, R., Fischer, J., Visbeck, M., & Karstensen, J. (2017). From interannual to decadal: 17 years of boundary current transports at the exit of the Labrador Sea. *Journal of Geophysical Research: Oceans*, *122*(3), 1724–1748. https://doi.org/10.1002/2016JC012271

Zhao, J., Bower, A., Yang, J., Lin, X., & Zhou, C. (2018). Structure and formation of anticyclonic eddies in the Iceland Basin. *Journal of Geophysical Research: Oceans*, *123*(8), 5341–5359. https://doi.org/10.1029/2018JC013886

Zou, S. J., Lozier, S., Zenk, W., Bower, A., & Johns, W. (2017). Observed and modeled pathways of the Iceland Scotland Overflow Water in the eastern North Atlantic. *Progress in Oceanography*, *159*, 211–222. https://doi.org/10.1016/j.pocean.2017.10.003

References From the Supporting Information

Meincke, J. (1978). On the distribution of low salinity intermediate waters around the Faroes. *Deutsche Hydrographische Zeitschrift*, *31*(2), 50–64. https://doi.org/10.1007/BF02226000

Ullgren, J. E., Fer, I., Darelius, E., & Beaird, N. (2014). Interaction of the Faroe Bank Channel overflow with Iceland Basin intermediate waters. *Journal of Geophysical Research: Oceans*, *119*(1), 228–240. https://doi.org/10.1002/2013JC009437